

Sub-millimetre observations of the Hubble Deep Field and Flanking Fields

S. Serjeant^{1,2}, J.S. Dunlop³, R. G. Mann³, M. Rowan-Robinson¹, D. Hughes⁴,
A. Efstathiou¹, A. Blain⁵, M. Fox¹, R. J. Ivison⁶, T. Jenness⁷, A. Lawrence³,
M. Longair⁸, S. Oliver⁹, J.A. Peacock³

¹ *Astrophysics Group, Blackett Laboratory, Imperial College, Prince Consort Road, London SW7 2BW, UK*

² *Centre for Astrophysics and Planetary Science, School of Physical Sciences, University of Kent, Canterbury, Kent, CT2 7NZ, UK*

³ *Institute for Astronomy, University of Edinburgh, Royal Observatory, Blackford Hill, Edinburgh EH9 3HJ, UK*

⁴ *Instituto Nacional de Astrofísica, Óptica y Electrónica (INAOE), Apartado Postal 51 y 216, 72000 Puebla, Pue., Mexico*

⁵ *Institute of Astronomy, University of Cambridge, Madingley Road, Cambridge CB3 0HA, UK*

⁶ *UK ATC, Royal Observatory, Blackford Hill, Edinburgh EH9 3HJ*

⁷ *Joint Astronomy Centre, 660 N. A'ohoku Place, Hilo, Hawaii 96720, USA*

⁸ *Cavendish Astrophysics Group, Cavendish Laboratory, Madingley Road, Cambridge CB3 0HE, UK*

⁹ *Astronomy Centre, CPES, University of Sussex, Falmer, Brighton BN1 9QJ, UK*

Accepted; Received; in original form 2001 May 22

ABSTRACT

We present an extended analysis of the SCUBA observations of the Hubble Deep Field (HDF), expanding the areal coverage of the Hughes et al. 1998 study by a factor of ~ 1.8 and containing at least three further sources in addition to the five in that study. We also announce the public release of the reduced data products. The map is the deepest ever made in the sub-millimetre, obtained in excellent conditions (median $850\mu\text{m}$ optical depth of 0.16). Two independent reductions were made, one with SURF and the other with a wholly algorithmic IDL analysis which we present in detail here. Of the three new sources, all appear to be at $z \gtrsim 0.9$ and one is provisionally associated with an Extremely Red Object ($I - K > 5$). There appears to be no significant cross-correlation signal between the $850\mu\text{m}$ fluctuations and sources detected by ISOCAM, the VLA or Chandra, nor with Very Red Objects ($I - K > 4$), nor quasars and quasar candidates in the HDF (notwithstanding a small number of individual weak candidate detections). This is consistent with interpretations where the $850\mu\text{m}$ -selected galaxies are at higher redshifts than those currently probed by ISOCAM/VLA, and predominantly not Compton-thin AGN. There are only one or two compelling cases for the radio source being the sub-mm source. Nevertheless, most SCUBA-HDF point sources have a nearby radio source apparently well-separated from the sub-mm centroid.

Key words: cosmology: observations - galaxies: formation - infrared: galaxies - surveys - galaxies: evolution - galaxies: star-burst - galaxies: Seyfert

1 INTRODUCTION

Sub-millimetre blank-field surveys represent a major time investment on the JCMT (e.g. Barger et al. 1999a,b, Lilly et al. 1999a,b, Eales et al. 1999, 2000,

Fox et al. 2002, Scott et al. 2002), and will arguably be among the most important extragalactic surveys of the coming decade. Lensing cluster surveys (e.g. Smail, Ivison & Blain 1997) demonstrated early on

the feasibility of sub-mm surveys with SCUBA (Holland et al. 1999) on the JCMT, and the extremely deep integration in the HDF by ourselves (Hughes et al. 1998) showed that sub-mm surveys are also feasible in blank fields. A total of 50 hours were spent in the HDF, and the central $90''$ radius portion of this data has already been presented in Hughes et al. (1998); here we present the results from the remainder of the map, extending substantially into the Hubble Flanking Fields (HFF), and announce the public release of the reduced data products.

This paper is structured as follows. In Section 2 we review the observing strategy and data acquisition; Section 3 discusses our data reduction algorithms and considers the source astrometry and flux calibration uncertainties (Section 3.2). Section 4 presents the results of our reductions, discusses the possibility of spatially correlated noise (Section 4.1), and presents a discussion of the source extraction (Section 4.3). Details of the data products in public release are presented in Section 4.4. In section 5 we cross-identify our point sources with HDF/HFF, ISO, Chandra and VLA sources, and discuss the ambiguities with identifications of sub-mm survey point sources. We also attempt to obtain statistical sub-mm detections of sources not detected individually. Finally, in Section 6 we summarise our results.

2 DATA ACQUISITION

Details of the observations were presented in Hughes et al. (1998); we summarise the main points here. We observed the Hubble Deep Field (HDF) with the Submillimetre Common User Bolometer Array (SCUBA) at the James Clerk Maxwell Telescope. We used the 64-point jiggle pattern to obtain Nyquist sampled images at both $450\mu\text{m}$ and $850\mu\text{m}$. We took a total of $88 \sim 1$ hour integrations on the HDF. The chop throw was set to $30''$ for ~ 48 hours, and the remainder was spent using a chop throw of $45''$. This observational strategy was intended as an experiment in minimising the sky fluctuation noise, but in retrospect it was fortunate since it gives powerful deconvolution constraints (Hughes et al. 1998). There was a bug in the telescope chop tracking software at the time, to the effect that the position angle of the chop varied throughout each integration, though the variation has since been quantified and its cause is well-understood. The resulting effective point spread function for the combined chop throws is plotted in Figure 1.

Of the 130 SCUBA-HDF demodulated data sets, only one (UT date 19980211 run 59) was affected by the astrometric shift caused by the clock error on the acquisition computer (Jenness 2000). This dataset has a pointing shift of $24''$ (possibly indicating a rotation error rather than clock shift), and has been excluded from the analysis below. The maximum offset for the remaining 129 demodulated data files is only $0.08''$.

Of the 265 calibration observations, six have shifts $> 1''$ (19980115 run 115, and 19980116 runs 66 – 68, 75, 76). These were excluded from the astrometric calibration below. The remaining calibrators all have shifts $< 0.13''$.

The integration time per point decreases rapidly towards the periphery of the field: Figure 2 shows the integration time as a function of position for the long wavelength detector array.

3 DATA ANALYSIS

3.1 Reduction algorithms

We made our reductions using SURF v1.2, the details of which are discussed in Hughes et al. (1998). In parallel we also reduced the data using a specially-written pipeline in the commercial Interactive Data Language (IDL) package, discussed briefly in Hughes et al. (1998). In this subsection we describe the pipeline more fully.

The IDL pipeline made a first-order fit to the two-dimensional sky background gradient before the combination of the nods. Combining the fit-subtracted nods gave a modest signal-to-noise improvement of $\sim 5\%$. Bolometer astrometry was obtained using the SCUBA2MEM routine developed by T.Jenness. The factory flat field was used, as in the SURF reduction. Extinction corrections for each bolometer were determined according to the current best practice (Archibald, Wagg & Jenness 2000) of using the smoothed CSO 225 GHz optical depths where available in conjunction with canonical conversions, or $850\mu\text{m}$ skydips to estimate the optical depths at $850\mu\text{m}$ and $450\mu\text{m}$ where the 225 GHz data are not available. This method of extinction correction has become standard practice in later versions of SURF but was not used in the Hughes et al. (1998) analysis. We used a 6th order polynomial fit to the archival 225 GHz data to model the short timescale variations, but used the skydips where less than 7 reliable CSO measurements are available within ± 1 hour of each observation.

Further differences between the SURF and IDL reduction algorithms are in the bolometer deglitching and sky subtraction. In the SURF reduction, noisy bolometers were identified and eliminated by hand, and an instantaneous sky level to be subtracted from the beamswitched data was determined from either a median level or from interactively-chosen bolometers. SURF also has the facility for timeline despiking. In the IDL pipeline, the approach was instead to iterate on the following procedure: (a) make noise estimates for each bolometer in 128-readout groups from Gaussian fits to the readout histograms; (b) perform an $N-\sigma$ clip deglitching using these time-dependent noise estimates; (c) determine and subtract a zero-point modal sky level in each readout from a fit to the readout histograms of all bolometers in the array. In

other words, each iteration makes a temporal noise estimate and deglitching, followed by a spatial sky subtraction. Each iteration performs successively harder deglitching cuts. Noisy bolometers are not eliminated by hand, but are instead automatically assigned a low inverse variance weight. This algorithm is not affected by the presence of sources, since there are no sources in the HDF field bright enough to be detected significantly in any single jigglemap, let alone readout. However, the same is not true of the calibrators. For finding glitches and determining noise levels in these, a timeline without object signal was constructed by subtracting the mean of the immediately previous and subsequent readouts from each readout. Our noise estimation is very different in philosophy and practice to (e.g.) the Canada-UK survey (e.g. Eales et al. 1999, 2000).

The final maps were constructed using an optimal noise-weighted drizzling algorithm (see Fruchter & Hook 1997), with the footprint set to 1 square arcsecond. (SURF also offers noise weighted mosaicing in the REBIN mosaicing routine, developed for the Hughes et al. 1998 HDF analysis, though the noise is estimated by a different algorithm.) In any square-arcsecond pixel, the flux is the noise-weighted average of the bolometer readouts at that position. As discussed above, the noise for each bolometer readout had been estimated from Gaussian fits to the readout histograms. The noise map was constructed in a similar fashion, with each pixel containing the formal error on the noise weighted average (i.e. $\sqrt{\Sigma(1/\sigma^2)}$). By the central limit theorem the noise statistics in our final map (as indeed in the REBINned equivalent) should be approximately Gaussian.

The 1'' footprint maps are an attempt to represent the detectors' views of the sky at each position. However the signal-to-noise per pixel is very low because the bolometers have been interleaved as far as possible rather than coadded, and no smoothing has yet been applied. For example, convolution with the point spread function is a very common method of extracting point sources (e.g. Eales et al. 1999, 2000 in the context of extragalactic sub-mm surveys) and is an optimal point source filter in the case of uniform noise. Here we discuss the non-uniform noise case.

To search for sources in the 450 μ m maps, we minimised the chi-squared of a Gaussian PSF fit with the instrumental FWHM (7'' at 450 μ m) at every position. This can be expressed as a convolution: if S is the image signal, P the PSF and W the reciprocal of the image variance, then the best fit flux F is given by:

$$F = \frac{(SW) \otimes P}{W \otimes P^2} \quad (1)$$

where \otimes denotes a convolution. The error on this best-fit flux is given by:

$$(\Delta F)^2 = \frac{1}{W \otimes P^2} \quad (2)$$

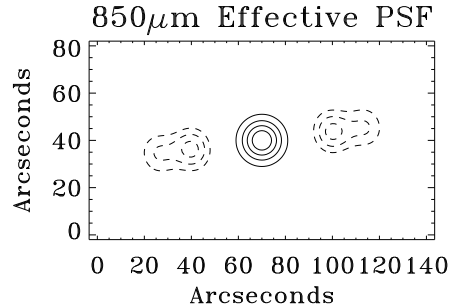


Figure 1. Effective point spread function at 850 μ m for the combined 30'' and 45'' chop throw data. Positive contours are in steps of 0.2 of the maximum, starting at 0.2. Negative contours (dashed) are in steps of -0.1 starting at -0.1 . North is up, and East to the left. The effect of the chop tracking bug is included.

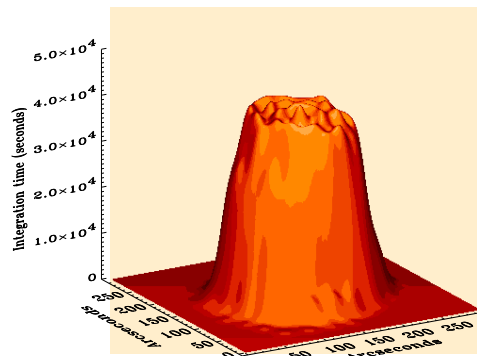


Figure 2. Integration time per 14.5'' FWHM beam at 850 μ m for the SCUBA-HDF. Note the steep sides and flat top.

(These relations are derived in the Appendix.) Setting a threshold in the $F/\Delta F$ map is formally optimal as a source extraction algorithm. Note that the $F/\Delta F$ map is not at all optimal for spatial resolution – in fact we have gained as much point source sensitivity as possible at the expense of spatial resolution in creating this map. Nevertheless, the centroids of the point sources are as accurately determined as possible in these maps. Since our sources are not expected to be resolved or confused at 450 μ m, the loss of spatial resolution is of no consequence. This algorithm has also been applied to our ongoing wide-area 850 μ m 8 mJy survey (Scott et al. 2002).

Extraction of sources in the 850 μ m map is more difficult, as the noise-weighted PSF convolution is only optimal if there are typically $\ll 1$ source per beam. This does not hold for the centre of the 850 μ m map (though the relative noise contribution of source

confusion drops strongly outside the area considered by Hughes et al. 1998). Instead we place model point sources at observed peaks, and by simultaneously varying their fluxes we minimise the total χ^2 of the map. Positions for these peaks were determined from the peaks in a noise-weighted convolution, though we also tried using the Hughes et al. (1998) CLEANed positions.

3.2 Calibration

In a beam map of Uranus taken during the run, the positions in the short and long arrays agreed to better than an arcsecond. CRL618, IRC+10216 and OH231.8 typically showed a slight ($\sim 2''$) shift between $450\mu\text{m}$ and $850\mu\text{m}$ positions, assumed intrinsic to the source. The $850\mu\text{m}$ position of CRL618 agrees with the corresponding NVSS position (accurate to only $5.7'' \times 3.8''$, Condon & Kaplan 1998), though the $450\mu\text{m}$ position lies just outside the 1σ VLA error box. The JCMT pointing grid is believed accurate to around $1''$. The IRAM 1.3 mm interferometric position determined by ourselves and others (Downes et al. 1999) is offset from our position of the brightest $850\mu\text{m}$ source by $2.5''$. This is a roughly 3σ discrepancy with the position published in Hughes et al. 1998 if we use $\pm\theta_{\text{FWHM}}/(2 \times S/N)$ as the astrometric uncertainty (where θ_{FWHM} is the beam FWHM and S, N are the signal and noise respectively), but it may be made consistent if the noise N includes a roughly equal confusion noise term added in quadrature (Hogg 2000), and/or a systematic error of order $1''$ in the JCMT pointing grid solution. Such a systematic could exist at the \sim arcsecond level in some parts of the azimuth–elevation plane and be consistent with existing inclinometry and pointing checks.

Flux calibration was obtained from planets and from CRL618, OH231.8 and IRC+10216. Using the peak flux of point sources in the $1''$ drizzling footprint IDL maps yields flux conversion factors of 223 ± 15 Jy/V at $850\mu\text{m}$ and 618 ± 115 Jy/V at $450\mu\text{m}$, where the errors have been estimated from the variance among the calibrators. These values are consistent with the advertised conversions valid at the time for the narrow-band filters.

4 RESULTS

4.1 Spatially correlated noise

The raw images with noise-weighted PSF convolutions are shown in Figure 3. The minimum noise level in the combined $30''$ and $45''$ maps is 0.39 mJy per beam, using a $14.5''$ FWHM Gaussian beam. Using the full beam profile (i.e., including the negative side-lobes) improves this by approximately $\sqrt{2/3}$. It is possible that some of the fluctuations in these images are spatially correlated, due to e.g. unsubtracted

structure in the (terrestrial) sky background. In order to quantify the level of this effect, we made a further parallel IDL reduction with the astrometry of the jiggle maps intentionally corrupted with arbitrary $n\pi/3$ rotations and/or reflections, and the offsets of the jiggle pattern reversed. Zero rotations were excluded. In mosaicing the jigglemaps to a final coadded image, a further arbitrary $n\pi/2$ reflection and/or rotation was added. Photometry observations were excluded from these mosaics, since the photometry targets lie on the invariant point of the rotations – i.e., the photometry observations are designed to have a bright source at the centre, so rotating the jigglemap around its centre would not smear out the source. These transformations will have the effect of smearing out genuine extragalactic sky structure, while preserving the noise level due to short-term terrestrial sky fluctuations. These corrupted maps therefore place an upper limit on the level of spatially correlated noise. No point sources were evident in these corrupted maps to a level of 4σ . We measured the 1σ fluctuations by iterative Gaussian fits to the main part of the maps, and found the flipped maps to have almost exactly the same noise level ($\sim 1\%$ higher in the flipped map). As a further comparison, randomising the individual bolometer astrometry yields an estimate of the spatially *uncorrelated* component, which gave a 1σ noise $\sim 1\%$ lower than the uncorrupted data, implying the noise is spatially uncorrelated to high precision. The fluctuation histograms for the $30''$ chop throw maps are shown in Figure 4; note the Gaussian nature of the corrupted maps.

4.2 Cirrus noise

How much of the fluctuations in the SCUBA-HDF maps (Figure 3) are due to cirrus noise? To estimate this, we need to know the power spectrum of cirrus fluctuations on scales down to the beam size. The power spectrum is observed to have a steep k^{-3} slope from the largest spatial scales probed by DIRBE (Wright 1998) to arcminute scales probed by IRAS and ISOPHOT (Gautier et al. 1992, Herbmeister et al. 1998, Lagache & Puget 2000). On sub-arcminute scales, the cirrus structure traced by extinction measured by ISOCAM (Abergel et al. 1999) continues the k^{-3} dependence to $\sim 6''$ scales, so that no characteristic scale has yet been detected for cirrus fluctuations.

Using the models of Gautier et al. (1992) with a k^{-3} power-law power spectrum at all scales, we obtain the following expression for the RMS $850\mu\text{m}$ cirrus fluctuations with a $45''$ chop throw:

$$\sigma_{850\mu\text{m}}(\mu\text{Jy}) \simeq 5I_{100}^{3/2} \quad (3)$$

where the cirrus $100\mu\text{m}$ background level I_{100} is given in MJy/sr, $\sigma_{850\mu\text{m}}$ is in μJy , and we have assumed $I_{100}/I_{850} = 14.2$ (Lagache et al 1999). Using $k^{-2.6}$ or $k^{-3.8}$ power spectra (the range spanned by the Gautier et al. models) modifies the numerical coefficient

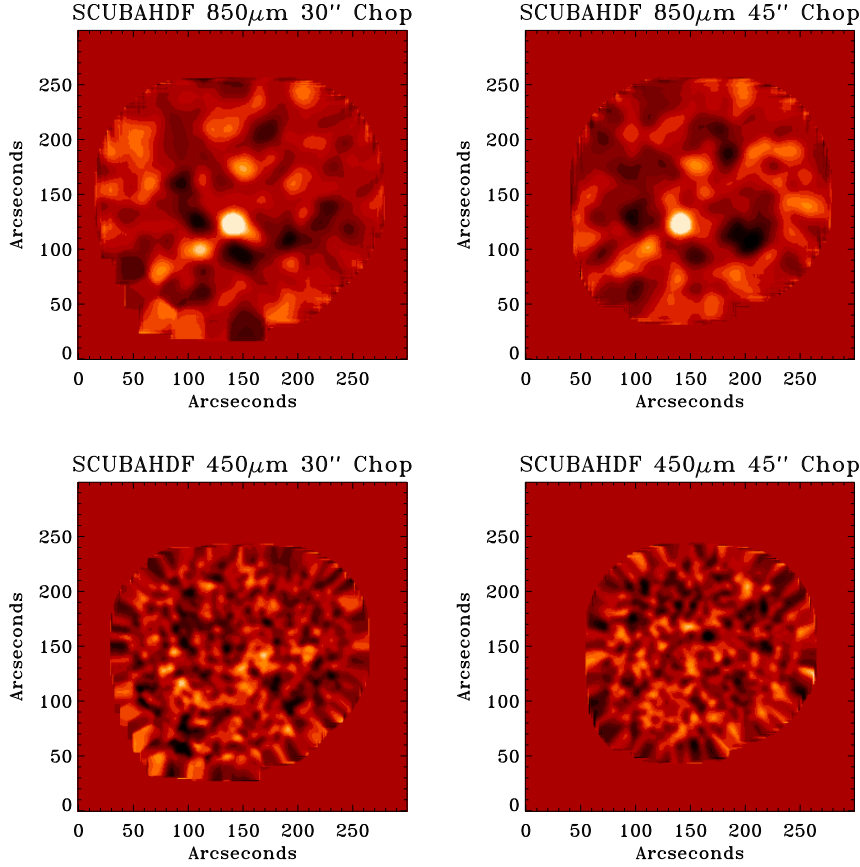


Figure 3. SCUBA images of the Hubble Deep Field prior to deconvolution. The $1''$ drizzling footprint images have been convolved with the positive part of the instrumental point spread function, using the noise-weighted convolutions given in equations 1 and 2 with P set to a Gaussian with FWHM of $14.5''$ at $850\mu\text{m}$ and $7''$ at $450\mu\text{m}$. Note that the maps are not fully-sampled at the edges. North is up, East to the left, and white indicates high flux values.

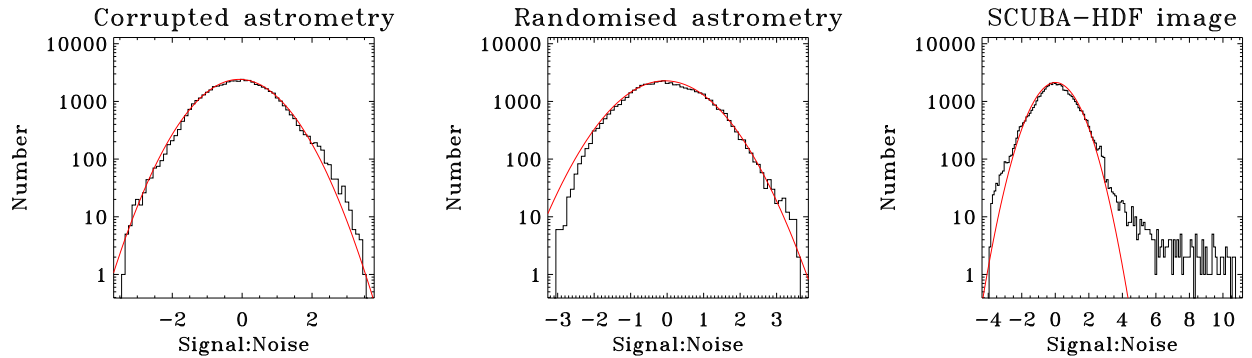


Figure 4. Fluctuation histograms for the $30''$ chop throw corrupted map (left), randomised map (centre), and the original $30''$ chop SCUBA-HDF map, all after a noise-weighted convolution with a $7.25''$ FWHM Gaussian (half the width of the JCMT primary beam). Iterative Gaussian fits were made to the histograms, rejecting outlying points, and are overplotted on the Figure. The means are consistent with zero and the variances with unity, as expected.

to approximately 11 or 1 respectively. Using a chop throw of $30''$ reduces the cirrus noise by $\sim 30 - 60\%$. Together with the $\times 2$ uncertainty in the power spectrum normalisation (corresponding to $\sqrt{2}$ uncertainty in the RMS noise), this expression should be correct to around an order of magnitude.

The IRAS Sky Survey Atlas (ISSA) gives an estimate of the I_{100} background in the HDF area. This obtains 0.25 ± 0.07 MJy/sr in a $30' \times 30'$ area centred on the HDF, consistent with the ($4'$ resolution) ISSA measurement at the HDF position itself of 0.331 MJy/sr. Neither value has been corrected for extragalactic background light contribution. These values are nevertheless slightly lower than the Schlegel et al. (1998) estimate of 0.61 MJy/sr.

In either case, the cirrus fluctuations at $850\mu\text{m}$ are negligible on the scale of the beam, and it can be similarly shown that the same applies at all sub-mm wavelengths for all current and future planned extragalactic sub-mm surveys on the beam scales, and on all scales in our SCUBA-HDF map according to the Gautier et al. models (e.g. Blain 1999).

4.3 Source extraction

4.3.1 Extraction algorithm

The $850\mu\text{m}$ map is close to the formal confusion limit (one source per 25-40 beams), so we cannot extract sources by simply convolving with the beam. Instead, in Hughes et al. (1998) we iteratively extracted sources using the CLEAN algorithm. Using numerical simulations we found that point sources were distinguishable from blends and confusion noise peaks by the fact that they appear at around the same position in both chop throw maps. Thus the number of claimed point sources in Hughes et al. 1998 is much lower than the number of distinct peaks found in the map. (Of course, this is not to say that none of the remaining peaks are real.)

Our approach here differs from the Hughes et al. (1998) analysis. Using the noise-weighted convolution peaks as a starting point, we make a simultaneous fit to both the chop throw maps. We simultaneously vary the fluxes (but not positions) of the point sources and obtain a solution minimising the total χ^2 . This procedure also naturally yields a signal-to-noise for each recovered source. This minimisation is discussed in more detail in Scott et al. (2002). Flux boosting caused by point sources being blended with neighbouring sources (i.e. boosting connected to confusion noise) is a possibility in our map (e.g. Eales et al. 2000; Scott et al. 2002; Borys et al. 2001), but one which depends on the clustering properties of the sources in question (e.g. Peacock et al. 2000). To avoid the source list being overly dependent on simulation assumptions we quote only fluxes uncorrected by boosting in this paper.

4.3.2 Comparison with Hughes et al. 1998

The results of this analysis are in general in excellent agreement with the analysis presented in Hughes et al. (1998), though certain subtle differences are worth noting. Firstly, our flux conversion factor is slightly different to that used in Hughes et al. (1998), resulting in a slightly lower flux for the brightest source. Secondly, the close pair of sources HDF850.4 and HDF850.5 were not deblended in this algorithm, although the combined “source” is clearly extended. Our CLEAN algorithm is more effective at deblending such pairs, so we adopt the flux ratio in Hughes et al. 1998 for these two sources. The χ^2 map using the sources at the CLEAN-deconvolved positions does not show obvious areas of poor fit. However, we caution that the map shows hints of a more complicated structure here. Thirdly, HDF850.3 appears rather fainter in the $45''$ chop throw map, so that it would fail the strict confirmation criterion used in Hughes et al. 1998. This particular source flux appears to be rather sensitive to the algorithm used to mosaic the map. The 1998 IDL analysis used a circular drizzling footprint of the same size as the bolometers, and the SURF map used the SURF REBIN task. The source appears in these to lie on a ridge of extended emission in these maps, which pushes it over the threshold. However in the current reduction using the $1''$ drizzling footprint, convolved with the beam, the ridge is less pronounced and the source drops below the threshold, to 2.1σ . The fact that the mosaicing and not the reduction is the key difference is confirmed by mosaicing the original 1998 SURF reduction with the current $1''$ drizzling footprint method: we again find the source below the threshold. In Table 1 we list the confirmed point sources found in both maps, with HDF850.3 in brackets for this reason.

4.3.3 Reliability and completeness

We tested our reliability and completeness by performing the source extraction on simulated maps. False positives were defined as sources extracted from the maps where no single simulated source within the beam contributes $> 50\%$ of the flux. Simulated sources were treated as missing if there was no extracted source within the beam with a flux within a factor of 2 of the simulated flux. We tried our source extraction using peaks from the maps convolved with a $14.5''$ beam, a $7.5''$ beam and a $5''$ beam. The results are shown in Figure 5. In this figure, sources are considered genuine if any single simulated source within the beam contributes $> 50\%$ of the observed flux. The reliability is defined as the fraction of extracted sources which pass this criteria for being genuine.

The results indicate that basing our fits on the peaks in the $14.5''$ map give the highest completeness and reliability, but unless the signal:noise cut is very high both only reach $\sim 80\%$. This reliability implies

Name	Position (J2000)		S_{850} (mJy)	S/N at 850 μ m	S_{450} (mJy)
HDF850.1	12 36 52.22	+62 12 26.5	5.6 ± 0.4	15.3	2.1 ± 4.1
HDF850.2	12 36 56.50	+62 12 03.5	3.5 ± 0.5	7.6	14.1 ± 5.5
(HDF850.3)	12 36 44.35	+62 13 07.5	1.0 ± 0.5	2.1	5.9 ± 4.3
HDF850.4	12 36 50.37	+62 13 15.9	$1.1 \pm 0.2^*$	5.1*	1.3 ± 4.0
HDF850.5	12 36 51.98	+62 13 19.2	$1.0 \pm 0.2^*$		0.6 ± 4.0
HDF850.6	12 37 01.21	+62 11 45.3	6.4 ± 1.7	3.8	-24 ± 54
HDF850.7	12 36 35.20	+62 12 42.4	5.5 ± 1.5	3.7	N/A
HDF850.8	12 36 53.07	+62 13 54.5	1.7 ± 0.5	3.5	-5.8 ± 5.7

Table 1. Sources from the 850 μ m map of the Hubble Deep Field. The quoted 450 μ m fluxes are the values at the quoted positions in the noise-weighted, beam-convolved 450 μ m map. HDF850.3 is included for consistency with the Hughes et al. (1998) paper, though it formally fails our revised source extraction algorithm. * = These two sources were detected as a single, blended source in the extraction algorithm. We have adopted the deconvolution of Hughes et al. (1998) to deblend these sources, and divided the total flux between the two according to the Hughes et al. ratio. The quoted signal-to-noise is for the combined source. HDF850.7 lies on the edge of the 850 μ m map and is not covered by the 450 μ m image.

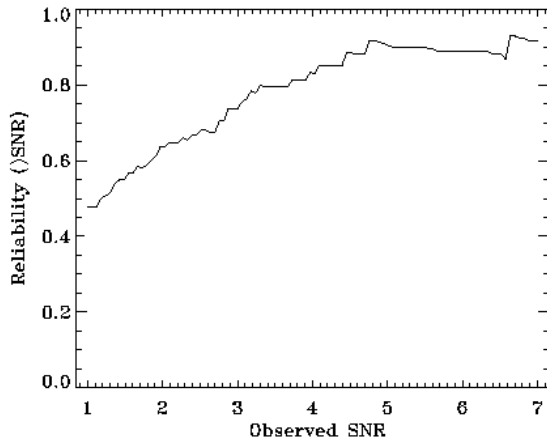


Figure 5. Reliability for the source extraction algorithm. Extracted sources were considered genuine if a simulated source lay within the beam and contributed at least 50% of the observed flux.

that of the 7 sources we extracted by this method, we expect 1.4 on average to be a blend. This agrees well with the fact that HDF850.4 and HDF850.5 from Hughes et al. (1998) are extracted as a single source, albeit extended. We adopt the CLEAN deconvolution from Hughes et al. (1998) to divide the flux for this source between the two. Nevertheless, we cannot exclude the possibility that our source list is entirely free of further blends.

No negative point sources were detected that were not associated with sidelobes of the positive sources.

4.3.4 Additional sources and structure in the map

The point sources selected for this χ^2 fitting were selected from the area covered by both the 30'' and 45'' chop data, because a simultaneous fit to both maps is intrinsic to our algorithm. However, one further source (HDF850.6) would pass the source extraction threshold if we require fitting in either map on its own. This source is just outside the area covered by the 45'' chop throw map and no useful limits can be obtained at its position from either 450 μ m map. The 30'' chop throw map is only just fully-sampled at this position. The source is on the periphery of the map where the effects of confusion are much less dominant, and the source is also identified in Section 5 with a VLA source and an extremely red galaxy. The VLA position is 2.8'' from the SCUBA centroid, and the shift is in the opposite sense to the shift between the Downes et al. (1999) IRAM position of HDF850.1 and the Hughes et al. (1998) SCUBA position of the same source. We therefore include this source in Table 1.

There is plenty of evidence for point sources outside the area of the map. For example, there is a $\sim 3\sigma$ feature in the vicinity of 123644+621420 in both chop throw maps, although the best-fit centroid is several arcseconds to the north off the edge of both maps. There is also an apparent trough of negative emission to the SW of the brightest source, seen in both chop throws. We carefully examined the individual jigglemaps to test whether this is due to an incorrectly-weighted noisy bolometer precessing around the jigglemap centre as each night's observations progressed. We found no evidence for such an effect in the individual jigglemaps (all of which appear to have Gaussian signal:noise histograms with unit variance); the apparent trough only appears in the coadded maps. This effect cannot be a Sunyaev-Zel'dovich decrement ($\lambda < 1.4$ mm) but can be attributed to confusion noise from the unresolved point sources (recall the negative

sidelobes of the beam). This serves to highlight the fact that our map contains much more information than the point sources extracted above.

In Figure 6 we show what amounts to a CLEAN reconstruction of our $850\mu\text{m}$ map. The point sources in Table 1 were first subtracted from each chop throw map using the theoretical PSF incorporating the SCUBA chop tracking bug. We coadded the $30''$ and $45''$ chop residual maps, and then convolved this combined residual map with a $7.5''$ FWHM Gaussian beam. Finally, we added $14.5''$ FWHM Gaussian beams to the convolved residual map at the positions of these sources, with $\sqrt{3/2} \times$ the peak flux of the original point sources, which approximates to the S:N gain in using the sidelobes. Thus, we effectively turn an $[-0.5, 1, -0.5]$ beam into simply $[\sqrt{3/2}]$.

4.3.5 $450\mu\text{m}$ sources

No sources were detected in the $450\mu\text{m}$ maps to a typical 4σ per beam depth of around 15 mJy, using a search for peaks in the noise-weighted convolved images. The $450\mu\text{m}$ fluxes at the positions of our $850\mu\text{m}$ sources are listed in Table 1. If the hint of a $450\mu\text{m}$ detection of HDF850.2 is real, this would place it at $(1+z)/(T/40K) = 2.0 - 5.1$.

4.4 Data release

We announce the public release of the reduced data to the community. These are available at http://astro.ic.ac.uk/elais/scuba_public.html, or from the authors. As well as the source lists quoted in this paper, the signal, noise and signal-to-noise maps at both wavelengths are available, for each chop throw separately and combined. Noise weighted point source convolutions are available for a variety of PSF widths. In addition, the parallel reductions with intentionally corrupted astrometry which quantify the level of spatially correlated noise, are also released as an IDL save set. We are also releasing the SURF-reduced products from our Hughes et al. (1998) analysis.

5 ASSOCIATIONS

In this Section we discuss the association of the 8 sources in Table 1 with objects detected in surveys of the HDF/HFF region undertaken in other wavebands; namely the optical surveys of Williams et al. (1996) and Barger et al. (1999c), the radio survey of Richards (2000) and the X-ray survey of Brandt et al. (2001).

In Figure 7 we present postage stamp images of the 8 SCUBA sources from Table 1. At the centre of each postage stamp we overlay, on an I_{814} band HDF or HFF image from Williams et al. (1996), the nominal 1σ positional error circle for the SCUBA

source, with a radius given by the conventional formula of $\theta_{\text{FWHM}}/2(S/N)$, where $\theta_{\text{FWHM}}=14.7$ arcsec is the FWHM of the beam at $850\mu\text{m}$ and S/N is the signal-to-noise ratio of the source detection, taken from Table 1. We note the names of nearby optical objects, from the catalogue of Williams et al. (1996) for the five sources (HDF850.1, HDF850.3, HDF850.4, HDF850.5, and HDF850.8) within the HDF and from that of Barger et al. (1999c) for the three HFF sources (HDF850.2, HDF850.6 and HDF850.7), and also mark the positions of VLA sources from Richards (2000) and Chandra sources from Brandt et al. (2001).

5.1 Possible SCUBA–VLA associations

One striking feature of this Figure is that five out of the eight sources lie within ~ 6 arcsec of a VLA source (three of which are also included in the deep Chandra catalogue of Brandt et al. 2001) which is a highly unlikely chance occurrence, given the low surface density of VLA objects on the sky. To quantify this, we may compute the probability $P_0 = 1 - \exp(-\pi N d^2)$ that the nearest object drawn from an unclustered population of surface density N (such as VLA objects at least as bright as the putative radio counterpart of the SCUBA source) should lie no further than d from the SCUBA source position under the assumption that the SCUBA and VLA source populations are uncorrelated. For the potential SCUBA–VLA associations with this set of five sources (HDF850.1, HDF850.2, HDF850.4, HDF850.6 and HDF850.7) the P_0 values so computed are 0.05, 0.03, 0.04, 0.01 and 0.01, respectively.

Similarly, Richards (1999) noted that as many as four of the five SCUBA–HDF sources from Hughes et al. (1998) could be identified with VLA sources from the 1.4 and 8.5 GHz catalogues of Richards et al. (1998) if the true positional errors in SCUBA source positions were significantly in excess of the nominal $\theta_{\text{FWHM}}/2(S/N)$ values. On the basis of associations between VLA J123656+621207 and HDF850.1, and between VLA J123649+621313 and HDF850.4, he advocated that the native SCUBA coordinate frame of Hughes et al. (1998) be shifted 4.8 arcsec to the West and 3.8 arcsec to the South. However, applying this offset has the effect of moving the two SCUBA sources that were initially the closest to their putative VLA identification much further from them: HDF850.2 and HDF850.6 are 4.2 and 2.9 arcsec, respectively, away from their nearest VLA source in the native SCUBA reference frame, but are both ~ 9 arcsec away once the shift advocated by Richards (1999) is applied, because their positions in Table 1 are already to the South and West of their supposed radio counterparts. In fact, no translation or rotation of coordinate frames can produce a good match between the positions of HDF850.1, HDF850.2, HDF850.4, HDF850.6 and HDF850.7 and all five of their respective possible ra-

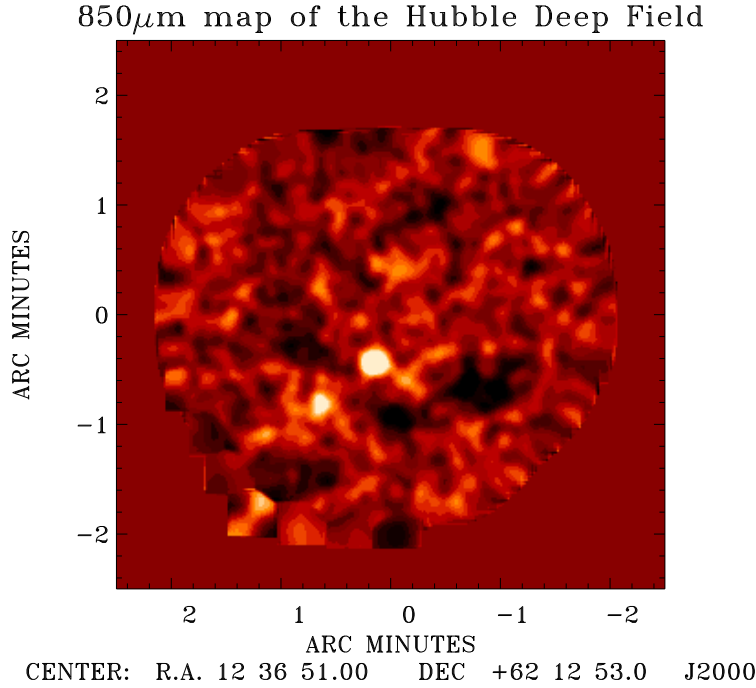


Figure 6. Deconvolved $850\mu\text{m}$ signal-to-noise map of the Hubble Deep Field. North is up, and East to the left. Note that the edges of the map are not fully-sampled.

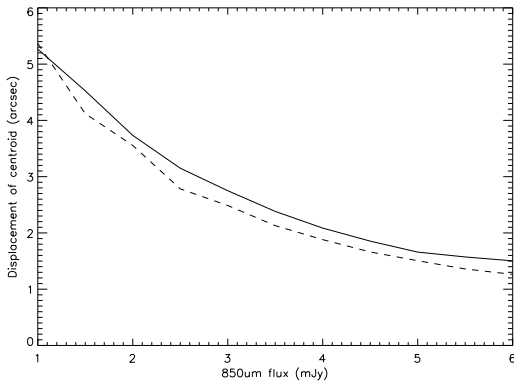


Figure 8. The effect of confusion noise on the positions of sources extracted from our $850\mu\text{m}$ map. The solid (dashed) line shows the mean (median) value of the distance between input and output source positions, as a function of the input flux of the simulated source.

radio counterparts, suggesting that there is not a systematic error in the native SCUBA coordinate frame of the sort deduced by Richards (1999) on the basis of the proximity of radio and submillimetre sources in the HDF.

Another possibility is that the confusion noise in the sub-mm map has significantly affected the positions of the sources we extracted from it, so we tested this using simulations. We selected six locations in the map well away from the locations of our eight detected sources, and defined at each a 5×5 square grid of

positions, with 6 arcsec separation between adjacent rows/columns. Then, one at a time, we placed a simulated source into the map at a grid position, and ran our source extraction routine on the resulting map, noting the displacement between the extracted source position and its input location. This process was repeated for simulated sources of a range of $850\mu\text{m}$ fluxes, so that we could measure how the effect of confusion noise varied with the S/N of the source detection. The results of this procedure are summarised by Figure 8 which plots the mean and median values of the distance between input and output source positions, as a function of the input flux of the simulated source. Assuming that there are no systematic differences between the input and output fluxes, we may then use our simulation results to estimate, for each of the five sources with putative radio counterparts, the probability that confusion noise could produce a positional offset as large as that required to reconcile the distance between the SCUBA and VLA positions. We find that, for HDF850.1, HDF850.2, HDF850.4, HDF850.6 and HDF850.7, the SCUBA–VLA offset corresponds to the 97th, 86th, 44th, 91st and 95th percentile, respectively, of the distribution of displacements produced by confusion at the relevant flux level.

It is perhaps conceivable that by avoiding bright sources in the map, our simulated sources will have suppressed confusion noise (if the clustering of the point sources is sufficiently strong). Indeed, the simulations of Eales et al. (2000) find large astrometric

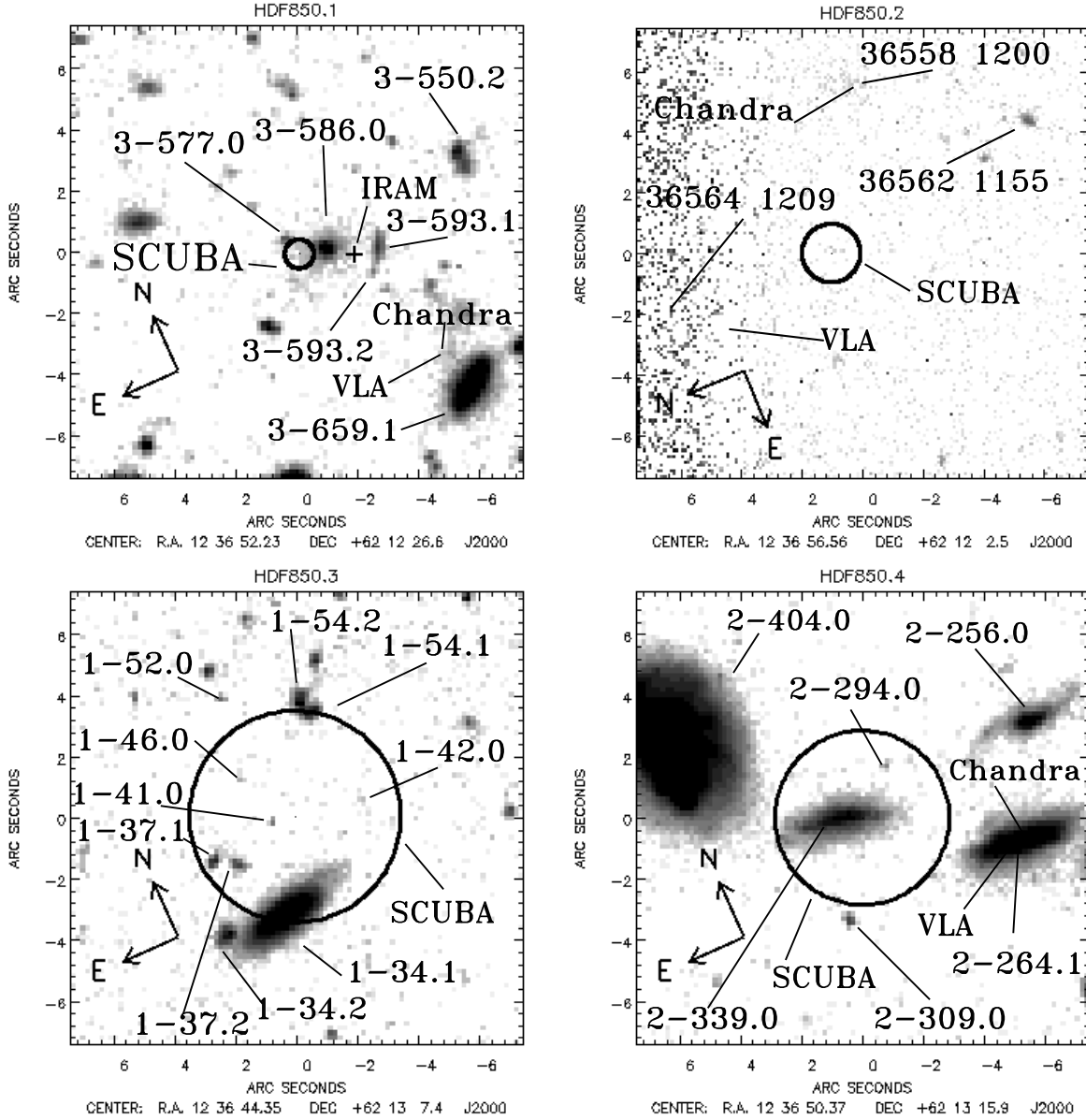


Figure 7. I_{814} band postage stamp images for the eight SCUBA sources from Table 1. The circle in the centre of each image is the nominal 1σ error circle for the SCUBA source, with radius equal to $\theta_{\text{FWHM}}/2(S/N)$, where $\theta_{\text{FWHM}}=14.7$ arcsec is the FWHM of the beam at $850\mu\text{m}$ and S/N is the signal-to-noise ratio of the source detection, taken from Table 1. (Note that we show in Section 5.1 that confusion leads this to underestimate the true astrometric uncertainties.) Also marked are the names of optical galaxies (from the catalogue of Williams et al. 1996 for HDF850.1, HDF850.3, HDF850.4, HDF850.5, and HDF850.8, and that of Barger et al. 1999c for HDF850.2, HDF850.6 and HDF850.7) and the locations of VLA sources from Richards (2000) and Chandra sources from Brandt et al. (2001).

shifts, albeit with very different mapping and source extraction algorithms. It is worth noting that the pointing solution of the JCMT has occasionally required revising with the appearance and discovery of new systematics (e.g. pointing shifts during transit), and although well-modelled the causes of these shifts are not all well-understood. Nevertheless, in the current absence of evidence to the contrary, we will treat

our simulations as accurately reflecting the astrometric uncertainties in our discussion of identifications.

We shall discuss below how the low P_0 values for the five possible VLA–SCUBA associations might have arisen, if these associations are incorrect, but we conclude from this subsection that neither a systematic shift in astrometric reference frame, nor the effect of confusion noise in our deep $850\mu\text{m}$ map, is sufficient

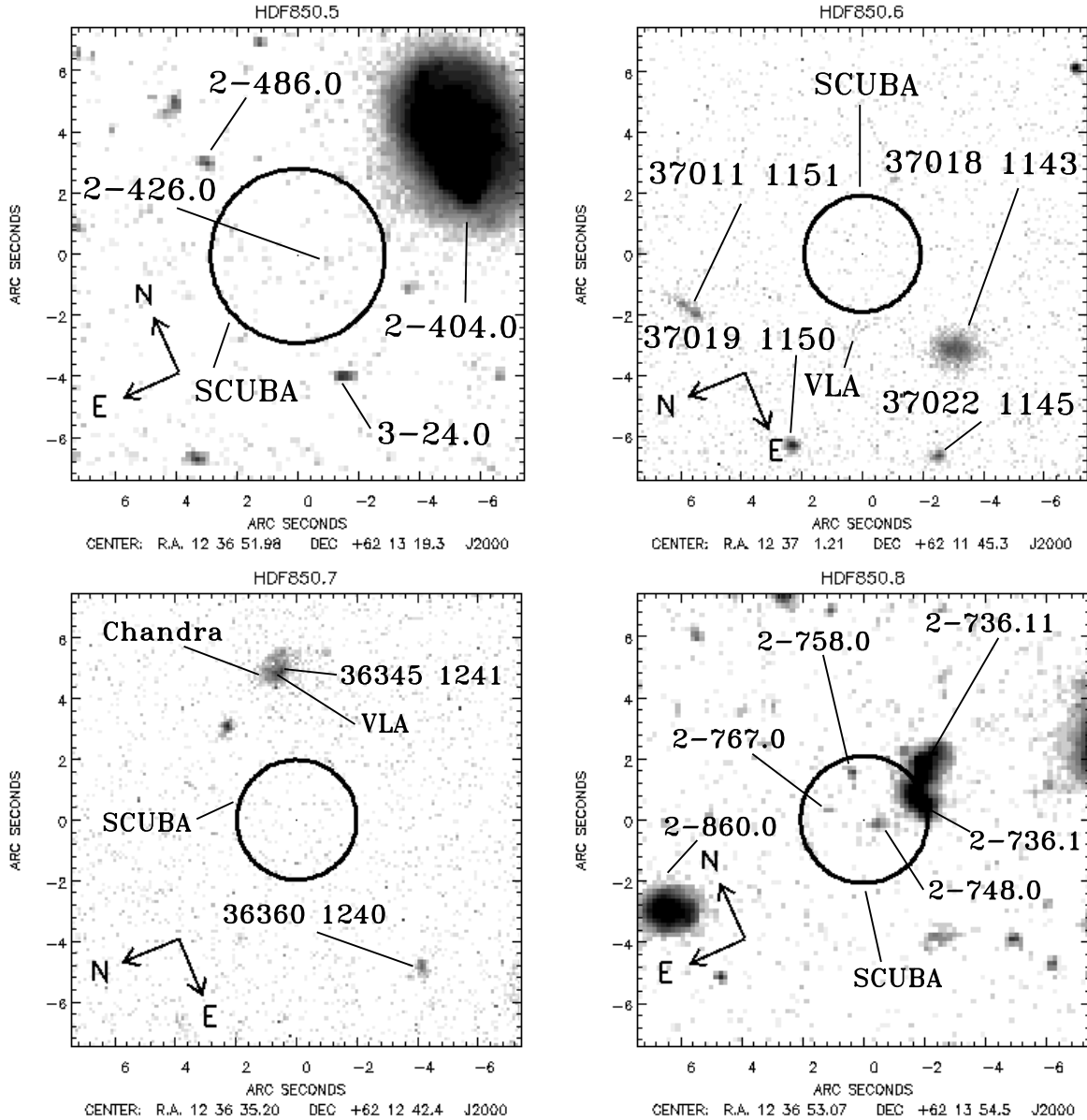


Figure 7 – *continued* I_{814} band postage stamp images for the eight SCUBA sources from Table 1. The circle in the centre of each image is the nominal 1σ error circle for the SCUBA source, with radius equal to $\theta_{\text{FWHM}}/2(S/N)$, where $\theta_{\text{FWHM}}=14.7$ arcsec is the FWHM of the beam at $850\mu\text{m}$ and S/N is the signal-to-noise ratio of the source detection, taken from Table 1. Also marked are the names of optical galaxies (from the catalogue of Williams et al. 1996 for HDF850.1, HDF850.3, HDF850.4, HDF850.5, and HDF850.8, and that of Barger et al. 1999c for HDF850.2, HDF850.6 and HDF850.7) and the locations of VLA sources from Richards (2000) and Chandra sources from Brandt et al. (2001).

to reconcile the displacements between the SCUBA and VLA positions of all of this set of five submillimetre sources and their putative radio counterparts. Furthermore, the accurate position for HDF850.1 measured by the IRAM interferometer (Downes et al. 1999) provides one case where we know for certain that the submillimetre source is not coincident with the nearby VLA source.

5.2 Methods for quantifying the reliability of identifications

The reliability of associations made between sources in one catalogue and objects in another are typically quantified using a simple Poisson method, working solely on proximity (as in computing the P_0 values above), or the likelihood ratio method, (e.g. Sutherland & Saunders 1992) which allows the inclusion of knowledge about the properties of the population un-

der study (e.g. flux or colour distributions, derived either from prior work or from the data themselves, if the sample size is large enough) enabling, for example, the further of two possible objects to be favoured if it matches more closely the properties of the expected counterpart being sought.

When the surface density of the object catalogue and/or the search radius is large, the simple expression for P_0 quoted above does not give a good estimate of the probability of such an extreme event (i.e. that an object so bright should be found so close to the source) occurring by chance in the Poisson model, as shown by Downes et al. (1986). If one searches a catalogue with magnitude limit m_{lim} out to a radius r_s from a source position, then the expected number of events as extreme as an association with an object of magnitude m at a distance d from the source is not simply equal to $E_0 = \pi d^2 N(\leq m)$, where $N(\leq m)$ is the surface density of objects at least as bright as magnitude m , and so the Poisson model probability of this event occurring by chance is not $P_0 = 1 - \exp(-E_0)$. This is because *a posteriori* probabilities at least as low as P_0 could have also been produced by there being objects brighter than m lying at distances greater than d from the source, or by objects fainter than m lying closer than d . The true *a priori* expected number of events as extreme as the putative association is then $E = E_0 + E_1 + E_2$, where E_1 and E_2 account for brighter/farther and fainter/closer objects respectively: i.e. $E_1 = \int_d^{r_s} N[\leq m_{\text{max}}(r)] 2\pi r dr$ and $E_2 = \int_m^{m_{\text{lim}}} n(m) dm \int_0^{r_{\text{max}}(m)} 2\pi r dr$, where $n(m)$ is the differential number density and where $N[\leq m_{\text{max}}(r)]$ and $r_{\text{max}}(m)$ are defined such that $\pi r^2 N[\leq m_{\text{max}}(r)] = E_0$ and $\pi N(\leq m) r_{\text{max}}^2(m) = E_0$, respectively.

As shown by Downes et al. (1986), this means that the *a priori* probability is given by $P = 1 - \exp(-E)$, where E takes the form $E = E_0[1 + \ln(E_c/E_0)]$, with $E_c = \pi r_s^2 N(\leq M_{\text{lim}})$. This reduces to $P = P_0$ in the limit $E_c \ll E_0$, which holds for the case of the Richards (2000) radio survey (so we were correct in quoting just P_0 values above), but does not hold for deep optical surveys of the HDF/HFF, given their much higher $N(\leq M_{\text{lim}})$ values: it is clear that, for such surveys, the exact P values obtained will depend on the value of r_s used, and that a sensible choice for that must be made, on the basis of the assumed astrometric accuracy of the source catalogue.

A similar choice must be made when using the likelihood ratio method (e.g. Sutherland & Saunders 1992), as that explicitly includes a model for the probability distribution of offsets between source and object positions, which typically reduces to the positional error distribution of the source population. The likelihood ratio is defined by $LR(f, x, y) = q(f) \cdot e(x, y)/n(f)$, where $e(x, y)$ is the probability distribution for positional offsets,

(x, y) , between source and object [normalized so that $\int e(x, y) dx dy = 1$ with the integral being taken over all space], $n(f)$ is the surface density of objects per unit interval in flux, f , and $q(f)$ is the probability distribution function for an ensemble of sources, measured in the same passband in which the object catalogue is defined. More generally, $q(f)$ and $n(f)$ can be replaced by the corresponding quantities for some other property of the source and object populations, such as their colours, photometric redshifts, etc.

The quantity $q(f)$ is unknown unless associations have previously been found between an ensemble of similar sources and a catalogue of similar objects, or unless the samples under study are sufficiently large that $q(f)$ can be estimated with sufficient accuracy from the data themselves. Neither of these conditions are met when, as here, one is seeking associations for a restricted number of sources drawn from a population about which little is known. In similar circumstances, seeking associations for *ISO* sources in the HDF and HDF-S, Mann et al. (1997, 2002) took a constant value for $q(f)$, after comparing the magnitude distributions of objects near source positions to that for the object catalogue as a whole, thereby deducing a peak in $q(f)$ at $I \sim 21$. This told them that the effect of their taking a constant $q(f)$ would be to underestimate the likelihood ratio for associations made with objects near that magnitude, which they could bear in mind should there be such an object vying with another of a different magnitude for selection as the likeliest counterpart of a given source; in both studies, Mann et al. (1997, 2002) found no such cases, justifying their use of a constant $q(f)$.

In this case, the number of SCUBA sources is so low that nothing about $q(f)$ can be deduced from comparing the magnitude distributions in this way, but, since we cannot estimate it well from previous work, either, we are forced to take it to be a constant if we are to use the likelihood ratio method at all. This leaves the *LR* value undetermined up to a constant factor, so we must also follow Mann et al. (1997, 2002) in quantifying the reliability of associations made via this modified likelihood ratio method through the use of simulations, rather than using the algebraic methods of Sutherland & Saunders (1992) and/or Rutledge et al. (2000), which can only be applied when correctly normalised *LR* values are available. In this case we compute, for each association, the probability, P_{ran} , that a fictitious source placed at a random location in the region covered by the object catalogue would yield an *LR* value through association with any object in that catalogue as high as that for the putative identification.

With $q(f)$ taken to be a constant, the modified likelihood ratio method, coupled with simulations to compute P_{ran} , employs no additional information than the Poisson method, so the P and P_{ran} values they yield for a particular association should

be similar, given consistent choices for the search radius r_S in the Poisson model and the value of σ in the Gaussian $e(x, y)$ positional error model used in the likelihood ratio method. One slight difference is that our likelihood ratio method uses $n(f)$, the differential flux distribution of the object catalogue, while the Poisson model employs the integral distribution, $N(\leq m)$. The use of the former may yield more robust results for bright optical IDs in situations where the image analyser producing the object catalogue splits bright objects into multiple “children” in a manner that is not readily accounted for across a sizeable catalogue, like that of Williams et al. (1996). To help assess the effect this might have on our results, we consider the SExtractor (Bertin & Arnouts 1996) catalogue available from the HDF-S WWW page (www.stsci.edu/ftp/science/hdfsouth/catalogs.html) and which we denote by N98, in addition the original catalogue of Williams et al. (1996, denoted W96), which was produced by a modified version of FOCAS (Jarvis & Tyson 1981) and the much shallower catalogue of Barger et al. (1999c, B99). In general, we do find that the likelihood ratio model does produce more consistent results from the different catalogues, that the Poisson method yields higher random probabilities than the likelihood ratio method, and that the differences between results are greater at brighter magnitudes, all consistent with the idea that these effects arise from the imperfectly-corrected over-splitting of bright objects.

5.3 Association results for individual sources

In this subsection, we quote both P and P_{ran} values for possible identifications of individual SCUBA sources with objects in optical and radio catalogues. When interpreting these values, the reader should bear in mind the assumptions behind them, both those inherent to the two methods [e.g. that the object population is unclustered] and those specific to their implementation here (e.g. taking $q(f)$ to be a constant, the choices made for r_S and σ , based on the estimated astrometric accuracy of the source positions, and possible object-splitting problems at bright magnitudes), and should note that the results for particular values of r_S and σ are not always directly comparable.

5.3.1 HDF850.1

For the present purposes, we assume that the correct position of this source is that of the IRAM 1.3mm source detected by Downes et al. (1999). That is a distance of 1.9 arcsec from the position quoted in Table 1, corresponding to the 69th percentile of the distribution of positional offsets estimated in the simulations of Section 5.1. We refer the reader to Downes et al. (1999) for a more detailed discussion of the possible

associations with this source; nothing in our analysis conflicts with their conclusions, although we do present here information from studies of the HDF region that have appeared since the publication of that paper.

The sub-arcsecond accuracy of the IRAM position confirms that the submm source is not the same object as the radio/X-ray source close to optical galaxy 3-659.1 (at a distance of 4.7 arcsec, that is at the 95th percentile of the distribution of positional offsets), although its position is consistent (Downes et al. 1999) with the tentative (4.5σ at 3cm) VLA source 3651+1226 in the supplementary list of Richards et al. (1998). At first sight there are two plausible optical counterparts: 3-586.0 is an $I_{814}(AB) \simeq 24$ galaxy 1.0 arcsec away (34th percentile), while 3-593.1 is slightly closer (0.8 arcsec, 27th percentile) but fainter $I_{814}(AB) \simeq 26$. For 3-593.1, the likelihood ratio method yields P_{ran} values of 0.15 and 0.14 using the W96 and N98 catalogues, respectively, for an assumed SCUBA positional error distribution with $\sigma=1$ arcsec, rising to 0.36 and 0.39 for $\sigma=2$ arcsec, while for 3-586.0 the corresponding P_{ran} values are 0.09, 0.14, 0.05 ($\sigma=1$ arcsec) for the W96, N98 and B99 catalogues, and 0.20, 0.39, 0.13 for $\sigma=2$ arcsec: the Poisson model yields $P=0.2-0.3$ for both galaxies with both the W96 and N98 data, with $r_S = 3$ arcsec.

Downes et al. (1999) note that, with the appearance of an elliptical galaxy and with photometric redshift estimates in the range $1.0 \leq z \leq 1.2$, 3-586.0 is highly unlikely to be the source of the submm/mm dust emission detected by SCUBA and IRAM. Photometric redshift estimates for 3-593.1 are around $z \sim 1.7$ (matching an Scd template), and Downes et al. (1999) show that, taking that value, the SED of HDF850.1/3-593.1 would be similar to the ultraluminous infrared galaxy VII Zw 31, although it could be a lower luminosity source gravitationally lensed by 3-586.0 (which would be consistent with the lower P_{ran} values for the association of HDF850.1 with that galaxy), while the lack of a significant U_{300} detection means that it could lie at a higher redshift: Downes et al. (1999) note that the photometric redshift methods of Fernandez-Soto and Rowan-Robinson both yield (less well favoured, but not wholly implausible) local probability maxima in the range $2.5 \leq z \leq 3$, although the limit on its U_{300} magnitude is not sufficiently tight to be sure that it would satisfy the colour selection criteria of Madau et al. (1996) for $2 \leq z \leq 3.5$ galaxies.

Further redshifts constraints may be deduced from $\alpha_{1.4}^{350}$, the 350 GHz to 1.4 GHz spectral index defined by Carilli & Yun (1999, 2000), under the assumption that both the submillimetre and decimetric radio luminosities of these sources are proportional to the rate at which they form massive stars (e.g. Condon 1992). If we assume that HDF850.1 is the counterpart of the 8.5 GHz source VLA 3651+1226

(Richards et al. 1998), and we assume a radio spectral index of $\alpha = -0.8$, then we deduce a 1.4 GHz flux of $28\mu\text{Jy}$. From the ratio of this and its $850\mu\text{m}$ flux of 5.6mJy , we calculate that $\alpha_{1.4}^{350} = 0.96$ which, from Carilli & Yun (2000) implies $2.25 \lesssim z \lesssim 4$, while, if we use the analogous relationship derived by Barger, Cowie & Richards (2000) from a fit to the SED of Arp220, we obtain $z = 2.89$. The flux limit of the Richards (2000) 1.4 GHz catalogue is $40\mu\text{Jy}$, so, if we disregard the tentative association of HDF850.1 with VLA 3651+1226, we would deduce $\alpha_{1.4}^{350} \geq 0.89$, implying $z \gtrsim 1.75$ (Carilli & Yun 2000), not too inconsistent with the photometric redshift estimates for 3-593.1 discussed above.

Further evidence supporting the identification HDF850.1 with VLA 3651+1226 comes with the convincing detection of a very red ($I - K > 5.2$) host galaxy coincident with the IRAM and VLA positions (Dunlop et al. 2002). The proximity of the elliptical galaxy 3-586.0 implies a gravitational lens amplification of up to 6.4, discounting pathological lens/source alignments. On the basis of fits to all the existing multi-wavelength data, Dunlop et al. (2002) quote a redshift estimate of $z = 4.1 \pm 0.5$, consistent with the radio/sub-mm limits quoted above.

Although 3-586.0 is already ruled out as the source of the sub-mm emission, it remains associated in the sense of providing gravitational lens amplification of HDF850.1. This is a salutary lesson for the problem of associations with sub-mm point sources: low values of the P and P_{ran} statistics may indicate any of a number of physical associations with the sub-mm source, such as gravitational lensing, large-scale structure, or the physical co-location of the multi-wavelength emission.

5.3.2 HDF850.2

This source lies outside the HDF, so we can only seek optical associations with objects in the much shallower catalogue of Barger et al. (1999c), with limiting magnitude $I \sim 24$, and to this depth we find no plausible optical ID for HDF850.2: the nearest is the $I \sim 23$ galaxy 36564 1209, which lies 5.6 arcsec away from the SCUBA position, yielding P_{ran} values in the range 0.6–0.7 for a positional accuracy of 2–3 arcsec, as estimated from the simulations of Section 5.1. The radio source VLA J123656+621207 lies 4.2 arcsec away from the SCUBA position, corresponding to the 90th percentile of the distribution of offsets in the simulations of Section 5.1. Barger et al. (2000) report an $850\mu\text{m}$ flux of 2.5 ± 0.7 mJy at that position, consistent with the value given in our Table 1, though this is also consistent with the SCUBA source being separated from the radio source by $5.6''$. Barger et al. (2000) list the detection of an optical counterpart for the radio source with $B=26.2$, in addition to upper limits in a series of other bands ($\text{HK}' > 22.6$, $I > 25.3$, $R > 26.6$, $V > 26.4$, $U' > 25.8$), while, on the basis of

their radio/submillimetre spectral index method they deduce a redshift of $z = 1.8_{-0.5}^{+0.7}$.

5.3.3 HDF850.3

This SCUBA source has one of the larger positional uncertainties amongst our sample because of the low S/N of its detection: indeed, as noted above, it does not satisfy our revised source extraction criteria, and we include it here only for consistency with Hughes et al. (1998). The position we deduce for this source is about 5 arcsec to the north-east of that determined by Hughes et al. (1998), and this shift makes their preferred ID (1-34.2) much less likely: we compute P and P_{ran} values in excess of 0.9, indicating that it is highly likely that an $I_{814}(AB) \sim 24$ galaxy should be found within 5 arcsec of a SCUBA position by chance. Much lower random probabilities are computed for the brighter [$I_{814}(AB) \sim 21$] galaxy 1-34.1, which is 3.4 arcsec from the SCUBA position from Table 1, corresponding to the 24th percentile in the simulated offset distribution: for the W96, N98 and B99 catalogues, we compute $P_{\text{ran}} = 0.16, 0.20$ and 0.10 , respectively, for $\sigma = 2$ arcsec, and $0.16, 0.29$ and 0.14 , for $\sigma = 5$ arcsec. Richards (1999) reports that this galaxy has a 3σ radio detection at 1.4GHz, and that its level of $23\mu\text{Jy}$ is more than an order of magnitude lower than what would be expected on the basis of the FIR–radio correlation, should the SCUBA emission be associated with 1-34.1, given its spectroscopic redshift of 0.485 (Phillips et al. 1997). In fact, it would need to be a factor of ~ 30 times higher to match the canonical $\alpha_{1.4}^{350}$ relation of Carilli & Yun (1999) for a $z = 0.485$ galaxy, while, conversely, the Carilli & Yun (2000) relation suggests that the true association lies at $0.9 \lesssim z \lesssim 2.25$.

We conclude that the only plausible optical association for this source, should the SCUBA source be real, is 1-34.1, but that we do not judge this to be a very reliable identification, both because there is a moderately high probability (0.1–0.2) of the proximity of such a source occurring at random, and also because the low redshift of this galaxy should lead to a 1.4GHz flux ~ 30 times higher than is detected (cf. a factor of ~ 2 scatter in the $\alpha_{1.4}^{350}$ relation): the $\alpha_{1.4}^{350}$ relation implies $0.9 \lesssim z \lesssim 2.25$ for this source.

5.3.4 HDF850.4

Hughes et al. (1998) associated this source with the $I_{814}(AB) = 23$ galaxy 2-339.0, which lies only 0.8 arcsec away from the SCUBA source position listed in Table 1. This corresponds to the 2nd percentile of the simulated offset distribution, and both the likelihood ratio and Poisson methods yield probabilities of less than 0.1 that this association should occur by chance, given a positional accuracy of 2–3 arcsec. Richards (1999) prefers an association of this source with VLA J123649+621313, which lies 5.3 arcsec away (50th

percentile) and is clearly associated with the galaxy 2-264.1, which is also the optical counterpart of an X-ray source from Brandt et al. (2001). Barger, Cowie & Richards (2000) measure an $850\mu\text{m}$ flux of 1.0 ± 0.6 mJy at the position of VLA J123649+621313, which does not itself constitute a significant detection, but is not inconsistent with the flux quoted for HDF850.4 in Table 1 above.

The SEDs resulting from these two associations have been discussed by Cooray (1999), who compares them with an Arp220 model shifted, in the case of 2-264.1, to $z = 0.475$ (the spectroscopic redshift measured for it by Cohen et al. 1996), and to $z = 0.9$ for 2-339.0, for which Hughes et al. (1998) report photometric redshifts in the range 0.74–0.88. Cooray (1999) finds that the Arp220 model gives a good fit to the optical-to-submm SED data resulting from both possible associations with HDF850.4, but that the identification with 2-264.1 has the additional support as this agreement is extended into the radio through the detection of VLA J123649+621313 at a flux consistent with the Arp220 model. Conversely, and as noted by Richards (1999), the lack of a 1.4GHz detection of 2-339.0 is difficult to square with the radio–FIR correlation: the $\alpha_{1.4}^{350}$ relation of Carilli & Yun (1999) would predict a 1.4 GHz flux of $\sim 280\mu\text{Jy}$ for a galaxy at $z = 0.9$, seven times the flux limit of the Richards (2000) catalogue. As noted by Brandt et al. (2001), the detection of 2-264.1 by Chandra is consistent with its being a powerful starburst (its soft X-ray luminosity is ~ 5 times that of M82: Griffiths et al. 2000) rather than an AGN, while its 1.4–to–8.5GHz spectral index ($\alpha = 0.72 \pm 0.15$) is inconclusive.

In summary, the optical data strongly favour 2-339.0 over 2-264.1, but the lack of a radio detection for 2-339.0 is very difficult to reconcile with an Arp220-like SED at the redshift assumed by Hughes et al. (1998). One possible reason why there is a lower probability for the random association with 2-264.1 may be that the proximity of HDF850.4 and HDF850.5 has shifted the centroid of the former to the East, which takes it further from 2-264.1, thereby making that association seem less secure than it should. On balance, we favour the associated with 2-264.1, but cannot rule out that with 2-339.0 or the possibility that HDF850.4 has no optical counterpart to the depth of the W96 catalogue.

5.3.5 HDF850.5

As with HDF850.4, the proximity of these two sources might have significantly moved the centroid of this SCUBA source, however, in this case, the shift would have been towards the most likely optical ID, 2-404.0, so, if anything, we are likely to have over-estimated the plausibility of its being the optical counterpart to HDF850.5. Even with that caveat, 2-404.0 does not appear a very secure identification: it lies 6.6 arcsec from the position of HDF850.5 given in Table 1,

which corresponds to the 67th percentile in the offset distribution, for a source of its flux, and its redshift ($z = 0.199$ Lanzetta et al. 1996) is inconsistent with the lower limit of $z \gtrsim 0.75$ deduced by the method of Carilli & Yun (2000) on the basis of the lack of a 1.4 GHz detection above the $40\mu\text{Jy}$ limit of the Richards (2000) catalogue. Hughes et al. (1998) favoured an association with the $I_{814}(AB) = 29$ galaxy 2-426.0, which is only 0.9 arcsec from the SCUBA position, however, with a likely positional accuracy of no better than ~ 3 arcsec, there is a high probability (≥ 0.7) of that occurring by chance, and that would only be increased were the true position of HDF850.5 to lie further to the East than that listed in Table 1, should the proximity of HDF850.4 have caused a significant shift in the position of both sources. We conclude that there is no reliable identification for this source.

5.3.6 HDF850.6

This is the first of the new sources, detected beyond the region studied by Hughes et al. (1998). It lies outside the HDF, so our optical information is limited to the shallow catalogue of Barger et al. (1999c). The nearest object in that catalogue is 37018 1143, an $I = 21.87$ galaxy at a distance of 4.4 arcsec: that yields likelihood ratio random probabilities of $P_{\text{ran}} = 0.3 - 0.4$ for $\sigma = 2 - 5$ arcsec, and Poisson probabilities in excess of 0.2 for $r_s \geq 5$ arcsec, so this is not a likely identification.

HDF850.6 lies 2.9 arcsec from the radio source VLA J123701+621146: this distance corresponds to the 93rd percentile of the offset distribution for a source of this flux, but this region of our SCUBA map is unusually noisy, so the $850\mu\text{m}$ detection is made at $S/N < 4$, and it is quite likely that we have underestimated its true positional uncertainty. We adopt the radio source as the most likely identification. Barger et al. (2000) measure an $850\mu\text{m}$ flux of 4.7 ± 2.1 mJy at the location of VLA J123701+621146, which is consistent with that quoted in our Table 1 above, though as with HDF850.2 this does not itself prove the radio and sub-mm sources are cospatial. This radio source is itself associated (Alexander et al. 2001) with an Extremely Red Object (ERO) with $I-K > 5$, for which Cohen et al. (2000) report a spectroscopic redshift of $z = 0.884$, on the basis of their identification of a single detected emission line as $[\text{OII}]\lambda 3727$; this is just consistent with the lower limit to the source redshift determined by the radio/submillimetre spectral index method of Carilli & Yun (2000), on the basis of the association of HDF850.6 with VLA J123701+621146, which implies $0.9 \lesssim z \lesssim 2.25$. Alexander et al. (2001) also detect X-ray flux for this source in the Chandra map of Brandt et al. (2001) (it is not included in the catalogue of Brandt et al. 2001, because it falls below their significance threshold; Alexander et al. 2001 accept sources with a lower significance, where they are coincident with EROs) and they show that

the extant data for this galaxy (they plot the $850\mu\text{m}$ flux of Barger et al. 2000) are reasonably well fit by shifting the Silva et al. (1998) SED model for Arp220 to $z = 0.884$ and dividing its luminosity by 2.2. We conclude that this is the most likely association for HDF850.6, but cannot rule out the possibility that this SCUBA source has no optical counterpart to the limit of the Barger et al. (1999c) optical catalogue.

5.3.7 HDF850.7

For HDF850.7, the nearest candidate HFF identification is a $z = 1.219$ (Barger et al. 2000), $I = 22.3$ galaxy at a distance of 5 arcsec, which is the 98th percentile of the simulated offset distribution, given the source flux. This large displacement leads to a high random probability (>0.30 from both Poisson and likelihood ratio methods), although, as with HDF850.6, this is a noisy region of our map, so we are certainly under-estimating the positional uncertainty. (The radio source is offset by 2.5σ from the SCUBA centroid, assuming a sub-mm positional uncertainty of $\theta_{\text{FWHM}}/(2 * S/N)$.) This galaxy is a Chandra source and is identified with the ISO source HDF_PM3.3 (Aussel et al. 1999) with a $15\mu\text{m}$ flux of $363\mu\text{Jy}$. It is also the radio source VLA J123634+621241, with a 1.4GHz flux of $230 \pm 13.8\mu\text{Jy}$, from the Richards et al. (2000) catalogue. If this were the correct identification, the radio/submillimetre flux ratio method of Carilli & Yun (2000) would imply a redshift between $z = 0.6$ and $z = 1.7$, consistent with the spectroscopic redshift above. Barger et al. (2000) measure an $850\mu\text{m}$ flux of $2.1 \pm 2.3\text{mJy}$ at the position of VLA J123634+621241, which is not inconsistent with the flux for HDF850.7 listed in Table 1. If the association is not accepted, and there is no radio counterpart for HDF850.7 down to the 1.4 GHz flux limit of $40\mu\text{Jy}$ for the Richards (2000) catalogue, then the redshift range implied by the Carilli & Yun (2000) method would be $1.75 \lesssim z \lesssim 4$. We conclude that there is no secure identification for this source: an association with the $z = 1.219$ galaxy identified with the radio source VLA J123634+621241 cannot be ruled out on the basis of the $850\mu\text{m}$ flux measured at that position by Barger et al. (2000), although it has a high probability of being a chance occurrence (albeit under a simplistic noise model), and it is possible that HDF850.7 lies at $z \gtrsim 1.75$, with no optical counterpart to the depth of the W96 catalogue.

5.3.8 HDF850.8

This SCUBA source is 2.0 arcsec (13th percentile) away from 2-736.1, which seems to be one an interacting pair of galaxies, which has a spectroscopic redshift of $z = 1.355$ (Cohen et al. 1996). The random probabilities from the likelihood ratio method are quite low 0.05, 0.14, 0.07 for W96, N98 and B99 for $\sigma = 2$

arcsec, and the lack of a radio detection is consistent with this redshift, given the radio/submm correlation method of Carilli & Yun (1999), which implies $z \gtrsim 0.9$. We conclude that this is a likely identification for HDF850.8.

5.4 Summary of association results

Despite the appearance of a great deal more multi-wavelength data for the HDF/HFF region since the publication of our initial analysis of the SCUBA HDF (Hughes et al. 1998), it remains the case that we do not have secure optical/near-IR IDs for the majority of the $850\mu\text{m}$ sources in this field. Our two most secure such IDs (those for HDF850.8 and HDF850.1) lie at $z \geq 1$, one source (HDF850.2) seems securely identified with a VLA source in an optically-blank field believed to lie at $1.3 \lesssim z \lesssim 2.5$, while HDF850.4 (and possibly also HDF850.6 and HDF850.7) appear to be associated with $z < 1.5$ galaxies detected in both the radio and the X-ray (although none of the cases is beyond doubt) and with SEDs well fit by an appropriately redshift Arp 220 SED. The final two sources (HDF850.3, HDF850.5) have no likely identification at all, only $z \gtrsim 0.75$ redshift constraints, based on non-detections in the radio. The available redshifts and redshift constraints are listed in table 2, and are consistent with source count model predictions (e.g. Rowan-Robinson 2001).

It is interesting to note that, if we had adopted the strategy of selecting optically-faint ($I \geq 24$) radio sources as likely SCUBA sources, as advocated by Barger et al. (2000) and Chapman et al. (2001a,b), we would only have recovered two out of the eight sources, well below the 70 per cent success rate claimed for this technique by Chapman et al. (2001b). *Provided* we have not underestimated our astrometric uncertainties, this implies that this pre-selection method may lead to incompleteness in detecting the submillimetre source population. Furthermore, giving optically-faint radio sources a high prior probability of being the counterparts of SCUBA sources can lead to mistaken identifications. For example, the radio source VLA J123651.7+621221, which lies 4.7 arcsec from the position for HDF850.1 given in Table 1, has $I > 25.3$ (Barger et al. 2000) and yields a Poisson probability of $P_0 = 0.05$ of being found so close to the SCUBA position by chance: if we believed that optically-faint radio sources are likely to be associated with SCUBA sources, we might have accepted this as a very plausible identification, but the high positional accuracy of the IRAM detection of this source (Downes et al. 1999) tells us that VLA J123651.7+621221 cannot be the correct ID. The discovery of a lensed near-infrared counterpart (Dunlop et al. 2002) at the IRAM position further argues against this ID.

If we accept that the five original SCUBA sources from Hughes et al. (1998) are not all robustly identi-

fied with VLA sources from the Richards (2000) catalogue – in fact, we argue above that only two are – how can we understand the result of Section 5.1 that all five of them yield $P_0 \leq 0.05$ for association with objects in that catalogue? It is clear that the confusion noise in our deep SCUBA image does have a significant impact on the accuracy with which we can estimate the positions of extracted sources. However, this cannot be the main factor: even if our SCUBA source positions are offset by a few arcsec by this effect (as indicated by Fig. 8), the true P_0 values must still be very low, because the radio catalogue is so sparse ($\lesssim 1$ source per square arcmin). The situation we observe is reminiscent of that reported by Almaini et al. (2001), who noted that SCUBA sources in the ELAIS N2 field appear to trace the same large-scale structure as objects detected in their deep Chandra image of the same field, but not to be identified with them. Almaini et al. (2001) sought to explain their result by postulating that the SCUBA phase and the AGN phase in a galaxy’s evolution are not simultaneous, so that within the galaxy population at $z \sim 2$, say, there will be galaxies exhibiting both sets of classes of behaviour.

While qualitatively similar, there is a quantitative difference in scale between that result and ours here: the SCUBA–Chandra pairs discussed by Almaini et al. (2001) are typically tens of arcsec apart (their cross-correlation function is significantly positive to a separation of ~ 100 arcsec), while our SCUBA–VLA pairs are separated by less than 6 arcsec. One solution is that the deeper data available in the HDF/HFF region are probing further down the luminosity function than is happening in ELAIS N2 (this is certainly the case for the submillimetre and hard X-ray data, since, in both cases, favourable k -corrections mean that the flux–redshift relation is flat for a source of a given luminosity at $z > 1$), so the number densities of detected objects drawn from these populations are higher, and, therefore, the mean separation of nearest neighbours will be lower. More fundamentally, the identification of the SCUBA sources with a population exhibiting significant clustering invalidates one of the assumptions in both the Poisson probability estimation method and the assignment of P_{ran} probabilities in our implementation of the likelihood ratio association procedure: an assessment of how large an effect this is on the probabilities is very model-dependent, given existing knowledge of the SCUBA source population, so we shall not attempt it here.

5.5 Cross-correlations with near-IR, VLA, ISOCAM, Chandra, and AGN candidates

5.5.1 Cross-correlation statistics

We have already stressed the difficulties in extracting further discrete point sources in the $850\mu\text{m}$ map, due to the problems of confusion and blending. Nevertheless, the map still contains many further real (blended) peaks and positive flux. In Peacock et al. (2000) we showed that after subtraction of the point sources, the residuals in the $850\mu\text{m}$ map correlate well with the positions of HDF Lyman break galaxies. Do these fluctuations also correlate with other known populations? We consider the $15\mu\text{m}$ ISO sources of Aussel et al. (1999) and Serjeant et al. (2002 in preparation); the 1.4 GHz catalogue from Richards et al. (2000) and Garrett et al. (2000), and the subset with optical blank fields from Richards et al. (1999); the hard X-ray Chandra sources of Hornschemeier et al. (2000), Brandt et al. (2001) and Alexander et al. (2001); the AGN and AGN candidates of Jarvis & MacAlpine (1998), Conti et al. (1999), and Richards et al. (2000); and the deep NICMOS sources of Thompson et al (2000).

In order to find the best cross-correlation statistics, we made numerical simulations of SCUBA–HDF maps and tested the distributions of (a) unweighted means of the fluxes at the source positions, as performed in Peacock et al. 2000; (b) Kolmogorov–Smirnov (KS) test significances, comparing the flux distribution at the source positions from each catalogue with that of the whole map; (c) noise-weighted coadds of the fluxes at the source positions, using the noise estimates derived in equation 2. As controls, we performed the same cross-correlations on random positions. We assumed a source count model consistent with previous sub-mm survey data; the simulation results were not found to be sensitive to the choice of model.

The unweighted means correctly reproduced the means of the input source fluxes, as expected, even where the number of beams per source was of order unity. We also checked the frequency of false negatives (failure to detect an underlying signal) and false positives (apparent detection of a cross-correlation signal which was not input into the simulation). The unweighted means and KS tests both gave the expected level of false positives (provided the number of beams per source was $\gtrsim 1.5$), but suprisingly the noise-weighted control coadds gave far more false positives than expected. This may perhaps be due to neglecting the (unknown) level of source confusion as a noise term. In the following Sections we therefore avoid using noise-weighted coadds. As regards false negatives, there is a non-negligible level of false negative detections for both KS and unweighted means: for example, $< 40\%$ of simulations gave a $> 2\sigma$ detection where all the target sources had < 0.5 mJy.

Name	HDF/HFF ID name	$S_{1.4 \text{ GHz}}$ (μJy)	Other Photometry	Candidate ID z (and z constraint from $\alpha_{1.4}^{350}$)
HDF850.1	VLA J123651+621226	16 ± 4	$I = 23.40 \pm 0.05$ $H = 20.40 \pm 0.05$ $K = 19.39 \pm 0.03$ $S_{1.3\text{mm}} = 2.2 \pm 0.3\text{mJy}$ $S_{8.4\text{GHz}} = 7.5 \pm 2.2\mu\text{Jy}$	$z_{\text{phot}} \simeq 4.1 \pm 0.5$ ($z \gtrsim 1.7$)
HDF850.2	VLA J123656+621207	46.2 ± 7.9	$U' > 25.8$ $B = 26.22$ $V > 26.4$ $R > 26.6$ $I > 25.3$ $HK' > 22.6$	($z \gtrsim 1.3$)
(HDF850.3)	1-34.1 (?)	< 40	$U_{300} = 25.24$ $B_{450} = 23.60$ $V_{606} = 22.20$ $I_{814} = 21.22$	$z_{\text{spec}} = 0.485$ (?) ($z \gtrsim 0.9$)
HDF850.4	2-264.1	49.2 ± 7.9	$U_{300} = 24.92$ $B_{450} = 23.48$ $V_{606} = 22.24$ $I_{814} = 21.39$ $S_{0.5-8\text{keV}} = 1.5 \times 10^{-16} \text{ ergs/s}$ $S_{0.5-2\text{keV}} = 6.49 \times 10^{-17} \text{ ergs/s}$ $S_{2-8\text{keV}} = 1.71 \times 10^{-16} \text{ ergs/s}$	$z_{\text{spec}} = 0.475$ ($z \gtrsim 0.5$)
HDF850.5	–	< 40		($z \gtrsim 0.75$)
HDF850.6	VLA J123701 + 621146(?)	128 ± 9.9	$U' > 25.8$ $B > 26.6$ $V > 26.4$ $R = 25.73$ $I = 24.81$ $HK' = 20.14$ $S_{15\mu\text{m}} = 15 \pm 9\mu\text{Jy}$ $S_{0.5-8\text{keV}} = 1.4 \times 10^{-16} \text{ ergs/s}$ $S_{0.5-2\text{keV}} = 4 \times 10^{-17} \text{ ergs/s}$	$z_{\text{spec}} = 0.884$ ($z \gtrsim 0.9$)
HDF850.7	VLA J1236345 + 621241(?)	230 ± 13.8	$U' = 24.72$ $B = 24.08$ $V = 24.22$ $R = 23.25$ $I = 22.29$ $HK' = 19.10$ $S_{15\mu\text{m}} = 363_{-38}^{+79}\mu\text{Jy}$	$z_{\text{spec}} = 1.219$ ($z \gtrsim 0.6$)
HDF850.8	2-736.1	< 40	$U_{300} = 23.01$ $B_{450} = 22.38$ $V_{606} = 22.27$ $I_{814} = 22.00$	$z_{\text{spec}} = 1.355$ ($z \gtrsim 0.9$)

Table 2. Multi-wavelength identifications of the sub-mm sources in the Hubble Deep Field. A question mark in the HDF/HFF ID name column denotes an uncertain identification: see text for details. HST magnitudes i.e. ($U_{300}, B_{450}, V_{606}, I_{814}$) are from Williams et al. (1996) while the remaining optical/near-infrared magnitudes are from Barger et al. (2000) and Dunlop et al. (2002). Mid-infrared fluxes are from Aussel et al. (1999). X-ray fluxes are from Brandt et al. (2001) and Alexander et al. (2001). Radio fluxes are from the catalogue of Richards (2000), redshifts for candidate IDs are denoted by z_{spec} or z_{phot} for spectroscopic measurements or photometric estimates, respectively, while the redshift constraints in parentheses are derived from the sources' submillimetre-to-radio spectral index, according to the method of Carilli & Yun (1999, 2000). The lower bounds using this relation are more robust than the upper bounds due to the steeper slope of the spectral index vs. redshift relation at lower redshifts. Also, due to the uncertainty of several radio-sub-mm cross-identifications (exemplified by the cautionary case of HDF850.1, e.g. Dunlop et al. 2002), we only quote lower limits on the redshift from the submillimetre-to-radio spectral index.

Source	1.4 GHz position (J2000)	S_{850} (30'')	S_{850} (45'')	S_{450}	$S_{1.4\text{GHz}}$
VLA/WRST	12 37 01.574 +62 11 46.62	7.3 ± 2.0	N/A	-34 ± 51	128 ± 9.9
VLA/WRST	12 36 42.098 +62 13 31.42	0.32 ± 0.82	2.87 ± 0.94	-8.8 ± 7.7	467 ± 24.6
VLA/WRST	12 36 44.386 +62 11 33.10	0.1 ± 1.45	3.7 ± 1.7	82 ± 61	1290 ± 61.2
WRST	12 36 46.284 +62 12 36.03	0.71 ± 0.66	1.67 ± 0.72	2.0 ± 4.4	467
WRST	12 36 53.050 +62 11 37.67	-0.15 ± 0.87	2.90 ± 1.25	7.1 ± 13.1	73

Table 3. Most significant candidate detections of 1.4 GHz sources from Richards et al. (2000) and Garrett et al. (2000) in the 850 μm maps with the Hughes et al. (1998) sources subtracted. The first source is identified with HDF850.6 (table 1). The observed fluxes quoted are the flux per beam in the 850 μm maps at the positions of the sources, but are subject to source confusion and blending. The noise estimates are the instrumental and sky noise only, and do not include confusion noise or calibration error.

NICMOS ID	WFPC2 ID	z	S_{850}^{pred} (mJy)	SFR^{pred} M_{\odot}/yr	$L_{\text{bol}}^{\text{pred}}$ L_{\odot}	S_{850}^{obs} 30'' chop	S_{850}^{obs} 45'' chop
166.000	4-307.0	1.60	1.78	534.7	1.21×10^{12}	0.07 ± 0.68	0.90 ± 0.76
277.211	4-186.0	1.84	1.51	375.2	1.07×10^{12}	1.57 ± 0.66	1.20 ± 0.76

Table 4. The brightest NICMOS HDF galaxies from Thompson et al. (2000). These two are also the galaxies with the largest estimated star formation rates and largest estimated bolometric luminosities by Thompson et al., listed in columns 5 and 6 respectively. The quoted observed fluxes are from the 850 μm maps at each chop throw with the point sources from Hughes et al. (1998) subtracted. The observed fluxes quoted are the flux per beam in the 850 μm maps at the positions of the sources, but are subject to source confusion and blending. The noise estimates are the instrumental and sky noise only, and do not include confusion noise or calibration error.

5.5.2 Hard X-ray sources and AGN

Neither the CHANDRA mega-second sample nor the AGN cross correlations yielded significant detections at 850 μm or 450 μm , using KS tests and unweighted means. We can use this to derive limits on the average flux-flux ratios in the CHANDRA population, for which we obtain the 2σ limit $S_{850\mu\text{m}}/(S_X) < 6 \times 10^{14}$ mJy / (erg s $^{-1}$ cm $^{-2}$) for the 0.5 – 8keV band, or 7×10^{14} for the 2 – 8keV band. This implies the population dominating the hard X-ray background contributes less than 2mJy per square arcminute at 850 μm , i.e. < 15% of the 850 μm extragalactic background light. This in turn excludes models where the bulk of the sub-mm population are dust-enshrouded (Compton-thin) AGN, rather than luminous starbursts, as other authors have also noted (e.g. Hornschemeier et al. 2000).

5.5.3 Very red objects

We tested the Very Red Object (VRO, $I-K > 4$) catalogues of Alexander et al. (2001). After excluding the ERO in the neighbourhood of HDF850.6, no significant correlation was found with the VROs, whether Chandra-detected or not.

5.5.4 Decimetric radio sources

We next consider the 1.4 GHz sources in the Hubble Deep Field detected by the VLA and MERLIN. The entire 1.4 GHz catalogue of Richards et al. (2000) yielded a marginal ($\sim 2\sigma$) cross-correlation in both the 30'' and 45'' chop maps. In the 30'' chop throw

map this is due to a single detection, identified with HDF850.6. In the 45'' map however, this source is outside the 850 μm coverage and the signal is due partly to a 2.9 ± 0.9 mJy (3.0σ) detection of the 1.4 GHz source at 12 36 42.098 +62 13 31.42, with radio flux of $467 \pm 24\mu\text{Jy}$ (Table 3). Despite a comparable noise level at this position this source is *not* detected in the 30'' chop throw map. If this source is real, then the failure to detect this source in the 30'' map may be due to a negative noise spike at this position, or a chance blending with a PSF hole from a source 30'' distant. If this sub-mm detection is indeed real, the radio:sub-mm flux ratio implies $z < 0.75$. The upper bound would be inconsistent with the lack of a 450 μm detection at around 2.5σ , if adopting the lower bound to the 450 : 850 μm ratio Hughes et al. 1998. Barring these three VLA sources in Table 3, the remaining cross-correlation is weaker (1.9σ in the 45'' map, and 1.4σ in 30''). The preliminary deeper 1.4 GHz list of Garrett et al. (2000) yielded a slightly more significant cross-correlation: 2.5σ and 1.6σ at 45'' and 30'' respectively. The 45'' result dropped to 1.8σ on exclusion of the candidate VLA source detections in Table 3, and almost all of this tentative signal is due to two further candidate identifications. These are also listed in Table 3.

We can also obtain constraints on the 850 μm :1.4 GHz flux ratio. We obtain a limit on the mean 350 – 1.4 GHz spectral index of between 0.25 and 0.5, implying that the 1.4 GHz μJy population typically lies at redshifts $z < 1$ (Carilli & Yun 2000) in agreement with existing spectroscopy. This limit is not affected by the exclusion of the candidate detections of 1.4 GHz sources, although the significance

of the cross correlation drops below 2σ when making this exclusion.

We also attempted a cross-correlation with the subset of 1.4 GHz sources which are optical blank fields, from Richards et al. 1999. For this subset a $\sim 2\sigma$ cross-correlation signal was found, which we found to be due entirely to HDF850.6.

5.5.5 Mid-infrared sources

For the ISO sources, a $\sim 2\sigma$ cross-correlation signal was found, and is due to a correlation between the ISO sources and structures on the western edge of the $45''$ chop throw $850\mu\text{m}$ map. Curiously, such a correlation does not exist in the $30''$ map, despite comparable noise levels. Such a disagreement between the chop throw maps is not unexpected in our simulations, as the probability of false negatives is not negligible (see above). Curiously also, this mirrors the lack of 1.4 GHz statistical detections in this area of the $30''$ map (see above) as compared against the $45''$ map.

5.5.6 K-band sources

The 282 NICMOS sources of Thompson et al. (2000) cover an area less than one arcminute square, in which there are less than 70 beams at $450\mu\text{m}$ and < 20 at $850\mu\text{m}$. This high source density per beam makes the statistics used above unsuitable. Instead, we use the predicted $850\mu\text{m}$ fluxes of Thompson et al. to make simulated confused maps for each chop throw, and use an M82 SED model from Rowan-Robinson et al. (1997) together with the quoted photometric redshifts to make corresponding $450\mu\text{m}$ maps.

We find no correlation between the observed and simulated maps at $450\mu\text{m}$. At $850\mu\text{m}$ a weak correlation was found to be due entirely to NICMOS 277.211, which has the second-brightest predicted flux and appears to lie on a positive deflection in the $850\mu\text{m}$ map. After excluding this galaxy, we could find no correlations in any subsets of the remaining sample. The galaxies with the brightest $850\mu\text{m}$ predictions are listed in Table 4.

Interestingly, a KS test comparing the two measurements of the brightest two objects with the total combined flux distribution yields a probability of 0.074 that the distributions are the same. The mean flux is $1.0 \pm 0.15 \text{ mJy}$, not far from the predicted mean of 1.645 mJy . These both seem to suggest that there is real $850\mu\text{m}$ flux at the positions of the NICMOS galaxies with brightest $850\mu\text{m}$ predictions. However for NICMOS 277.211 the $850\mu\text{m}$ excess is due to a peak $\sim 6''$ distant from the candidate source in both maps, but with a position consistent to around $\sim 2''$ in the two maps. So, the $850\mu\text{m}$ flux may either be due to the NICMOS galaxy, or may be due to this (presumably) unrelated apparent peak $6''$ away. The latter possibility may be ascribed to the effects of confusion at this flux density level (Hogg 2000).

5.5.7 Summary of cross-correlations

None of the catalogues considered so far yielded a significant cross-correlation (barring individual point sources), whether in the separate chop throw maps or in the combined maps, at either wavelength. Although the probability of false negatives is not negligible, the fact that we repeatedly fail to find a cross-correlation signal suggests the SCUBA sources that comprise the sub-mJy fluctuations are on the whole distinct from the ISO, VLA and Chandra populations. This is consistent with the lack of point sources in common between hard X-ray and sub-mm sources, and with the source count model of Rowan-Robinson (2000), and suggests that both the $850\mu\text{m}$ background and point sources are dominated by star-forming galaxies at $z \gtrsim 1$, and not by lower redshift galaxies or AGN.

Elbaz et al. (2002) argue that a significant fraction of the $140\mu\text{m}$ extragalactic background light is due to the resolved $15\mu\text{m}$ galaxy population. Our cross-correlation results demonstrate that the $15\mu\text{m}$ galaxies cannot also be responsible for the $850\mu\text{m}$ background. This confirms the expectation from source count models (e.g. Rowan-Robinson 2001).

The lack of statistical cross-correlations, and point-source cross-identifications, is markedly at odds with the presence of the SCUBA sources having near neighbours from multi-wavelength populations. For example, we have already discussed the neighbouring 1.4GHz populations; in figure 9 we plot the positions of the SCUBA sources against the VLA blank fields (Richards et al. 1999) and the Chandra-detected VROs (Alexander et al. 2001). Despite the apparent presence of clear SCUBA cross-identifications with these Chandra and/or VLA sub-populations, one SCUBA source (HDF850.1) is demonstrably identified with neither.

6 CONCLUSIONS

Our publicly-available SCUBA map of the Hubble Deep Field resolves a substantial fraction of the extragalactic sub-mm background. At least half the sources appear to be at $z \gtrsim 1$, based on our preliminary identifications. The lack of statistical cross-correlation signals with ISO, VLA or Chandra sources implies that the sources detected in these surveys are different populations and/or at different redshifts, in turn implying the sub-mm galaxies at these flux densities are mainly high-redshift ($z > 1$) galaxies with bolometric luminosities dominated by star formation. We infer that the μJy radio population lies predominantly at $z < 1$, in agreement with existing optical spectroscopy, and that the populations dominating the hard X-ray background contribute $< 15\%$ of the sub-mm extragalactic background light. Only two out of eight sub-mm sources are robustly identified with VLA sources; radio pre-selection (e.g. Barger et al. 2000, Chapman et al. 2001a,b) would therefore have

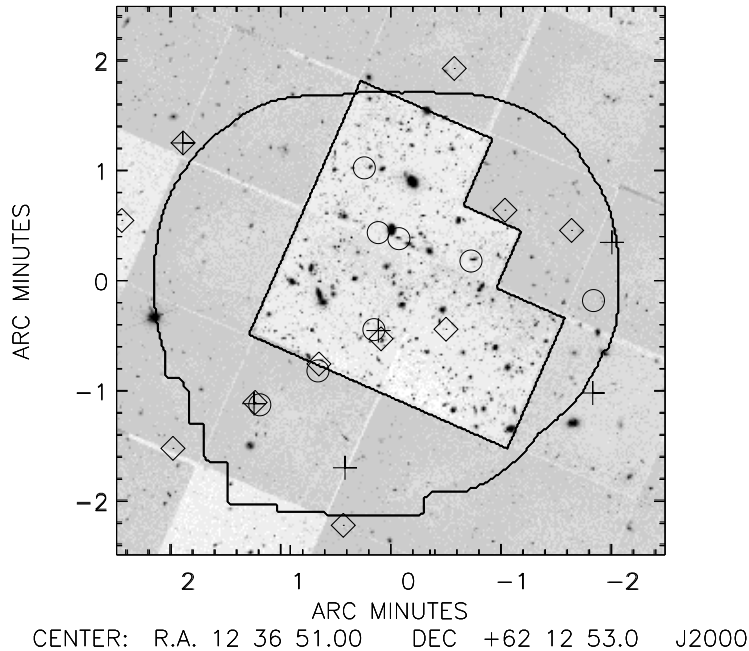


Figure 9. SCUBA-HDF sources (circles) overlaid on a mosaic of Hubble Flanking Field F814W images. The scale is the same as that of figure 6. The outer contour shows the areal coverage of the SCUBAHDF 850 μ m map, after convolution with the beam. The inner contour shows the areal extent of the Hubble Deep Field North. Also plotted are VLA sources with optical blank fields (Richards et al. 1999; diamonds), and Chandra-detected Very Red Objects (Alexander et al. 2001; crosses; n.b. distinct from the catalogue of Brandt et al. 2001). Despite appearances to the contrary, in at least one case (HDF850.1) the Chandra and/or VLA sources are demonstrably *not* identified with the sub-mm source.

recovered ≥ 2 out of the 8 SCUBA point sources in the HDF. Nevertheless, five of the eight sub-mm sources have radio sources much closer than would be expected by chance, but which are still not close enough to be physically identified with the sub-mm emission (provided we have not underestimated the astrometric uncertainties). Millimetre-wave interferometry has confirmed this is the case in the source HDF850.1, with a lensed near-infrared counterpart (Dunlop et al. 2002). This raises the interesting possibility that not all radio sources associated with sub-mm galaxies are responsible for the far-infrared emission. Unambiguous identifications have so far almost exclusively been obtained using interferometric mm-wave follow-ups of brighter sub-mm sources, reinforcing the strategy of wide-area, shallow sub-mm surveys for the study of the resolved sub-mm point source population (e.g. Scott et al. 2002, Fox et al. 2002).

ACKNOWLEDGEMENTS

This work was supported by PPARC (grant number GR/K98728). JD acknowledges the enhanced research time awarded by a PPARC Senior Fellowship. The James Clerk Maxwell Telescope is operated on behalf of the Particle Physics and Astronomy Research Council of the United Kingdom, the Nether-

lands Organisation for Scientific Research and the National Research Council of Canada. The authors acknowledge the data analysis facilities provided by the Starlink Project which is run by CCLRC on behalf of PPARC.

APPENDIX: NOISE-WEIGHTED SOURCE EXTRACTION

At every point (i, j) in the image we wish to determine the best fit (minimum χ^2) point source. Suppose the point spread function is $P(x, y)$, the image signal is $S(i, j)$, and the image noise is $N(i, j)$. The χ^2 at position i, j is

$$\chi^2(i, j) = \sum_{x, y} \left(\frac{S(i - x, j - y) - FP(x, y)}{N(i - x, j - y)} \right)^2 \quad (4)$$

where F is the best-fit flux at position (i, j) . If we minimise the χ^2 with respect to F we obtain

$$\frac{d\chi^2}{dF} = -2 \sum_{x, y} \frac{S(i - x, j - y) - FP(x, y)}{N(i - x, j - y)^2} P(x, y). \quad (5)$$

Setting this to zero and rearranging gives

$$F(i, j) = \frac{\sum_{x, y} S(i - x, j - y) W(i - x, j - y) P(x, y)}{\sum_{x, y} W(i - x, j - y) P(x, y)^2} \quad (6)$$

where $W = 1/N^2$ can be thought of as the weights.

This is equivalent to a convolution. We obtain the result that the best fit flux image is

$$F = \frac{(SW) \otimes P}{W \otimes P^2} \quad (7)$$

where \otimes denotes a convolution. Propagating the errors on F , we obtain

$$(\Delta F)^2 = \frac{1}{W \otimes P^2} \quad (8)$$

Note that a signal - to - noise map here ($F/\Delta F$) is not the same as a χ^2 map:

$$\frac{F}{\Delta F} = \frac{(SW) \otimes P}{\sqrt{W \otimes P^2}} \quad (9)$$

whereas

$$\begin{aligned} \chi^2 &= [(S/N)^2 \otimes (0 \times P + 1)] \\ &\quad + F^2(W \otimes P^2) - 2F[(SW) \otimes P] \\ &= [(S/N)^2 \otimes (0 \times P + 1)] - F[(SW) \otimes P] \end{aligned} \quad (10)$$

(the first step multiplies out eqn 4, and the last step is obtained by using the expression for F , eqn 7).

This method of source extraction is now also being used on the 1'' drizzling footprint images made for the ongoing 8 mJy 850 μ m survey by ourselves (Scott et al. 2002, Fox et al. 2002).

REFERENCES

- Abergel, A., André, P., Bacmann, A., et al., 1999, in *The Universe as seen by ISO*, ESA-SP 427
- Alexander D.M., Vignali C., Bauer F.E., Brandt W.N., Hornschemeier A.E., Garmire G.P., Schneider D.P., 2001, *AJ*, 122, 2156
- Almaini, O., et al., 2002, *MNRAS*, submitted (astro-ph/0108400)
- Archibald, E.N., Wagg, J.W., Jenness, T., 2000, JAC document SCD/SN/002, currently available at <http://www.jach.hawaii.edu/JACdocs/JCMT/SCD/SN/002/index.html>
- Aussel, H., Cesarsky, C.J., Elbaz, D., Starck, J.L., 1999, *A&A*, 342, 313
- Barger A.J., Cowie L.L., Richards E.A., 2000, *AJ*, 119, 2092
- Barger, A., Cowie, L.L., Sanders, D.B., 1999, *ApJL*, 518, 5
- Barger, A., Cowie, L.L., Smail, I., Ivison, R.J., Blain, A.W., Kneib, J.-P., 1999b, *AJ*, 117, 2656
- Barger, A.J., Cowie, L.L., Trentham, N., Fulton, E., Hu, E.M., Songalia, A., Hall, D., 1999c, *AJ*, 117, 102
- Bertin E., Arnouts S., 1996, *A&AS*, 117, 393
- Blain, A., 1999, in 'Photometric Redshifts and High Redshift Galaxies', R J Weymann, L J Storrie-Lombardi, M Sawicki, R J Brunner eds. *PASP conf series vol. 191*, p. 255-264 (1999) (astro-ph/9906141)
- Blain, A.W., Ivison, R.J., Kneib, J.-P., Smail, I., 1999, in 'The Hy-Redshift Universe: galaxy formation and evolution at high redshift', eds. A. J. Bunker & W. J. M. van Breughel, *ASP conference vol. 193* (2000). ASP: San Francisco, p. 246-249 (astro-ph/9908024)
- Blain, A., Longair, M., 1993, *MNRAS*, 264, 509
- Borys, C., Chapman, S., Halpern, M., Scott, D., 2001, preprint (astro-ph/0107515)
- Brandt W.N., et al., 2001, *AJ*, 122, 1
- Carilli, C.L., Yun, M.S., 1999, *ApJL*, 513, 13
- Carilli, C.L., Yun, M.S., 2000, *ApJL*, 539, 1024
- Chapman S.C., Richards E.A., Lewis G.F., Wilson G., Barger A.J., 2001a, 2001, *ApJL*, 548, 147
- Chapman S.C., Lewis G.F., Scott D., Borys C., Richards E.A., 2001b, astro-ph/0111157
- Cohen J.G., Cowie L.L., Hogg D.W., Songaila A., Blandford R., Hu E.M., Shopbell P., 1996, *ApJ*, 471, L5
- Cohen J.G., Hogg D.W., Blandford R., Cowie L.L., Hu E., Songaila A., Shopbell P., Richberg K., 2000, *ApJ*, 538, 29
- Condon J.J., 1992, *ARA&A*, 30, 575
- Condon, J.J., Kaplan, D.L., 1998, *ApJS*, 117, 361
- Conti, A., Kennefick, J.D., Martini, P., Osmer, P.S., 1999, *AJ*, 117, 645
- Cooray A.R., 1999, *New Astronomy*, 4, 377
- Désert, F. -X., Puget, J. -L., Clements, D.L., Péroult, M., Abergel, A., Bernard, J.-P., Cesarsky, C.J., 1999, *A&A*, 342, 363
- Downes A.J.B., Peacock J.A., Savage A., Carrie D.R., 1986, *MNRAS*, 218, 31
- Downes, D., et al., 1999, *A&A*, 347, 809
- Dunlop, J., et al., 2002, preprint, astro-ph/0205480
- Eales, S., et al., 1999, *ApJ*, 515, 518
- Eales, S., Lilly, S., Webb, T., Dunne, L., Gear, W., Clements, D., Yun, M., 2000, *AJ*, 120, 2244
- Efstathiou, A., Rowan-Robinson, M., Siebenmorgen, 2000, *MNRAS*, 313, 734
- Elbaz, D., Cesarsky, C., Chaniai, P., Aussel, H., Franceschini, A., Fadda, D., Chary, R., 2002, *A&A*, in press
- Fixen D.J., et al., 1998 *ApJ*, 508, 123
- Fox, M., et al., 2002, *MNRAS*, in press (astro-ph/0107585)
- Fruchter, A., Hook, R.N., 1997, in *Proc. SPIE Vol. 3164*, p. 120-125, Applications of Digital Image Processing XX, Ed. Andrew G. Tescher.
- Garrett, M.A., de Bruyn, A.G., Giroletti, M., Baan, W.A., Schilizzi, R.T., 2000, *A&A*, 361, L41
- Gautier, T.N., Boulanger, F., Péroult, M., Puget, J.L., 1992, *AJ*, 103, 1311
- Griffiths R.E., Ptak A., Feigelson E.D., Garmire G., Townsley L., Brandt W.N., Sambruna R., Bregman J.N., 2000, *Science*, 290, 1325
- Guiderdoni, B., Bouchet, F.R., Puget, J.L., Lagache, G., Hivon, H., 1998, *Nature* 390, 257
- Herbstmeier, U., Ábráham, P., Lemke, D., Laureijs, R.J., Klass, U., Mattila, K., Leinert, C., Surace, C., Kunkel, M., 1998, *A&A*, 332, 739
- Hogg, D.W., 2000, preprint astro-ph/0004054
- Holland, W.S., et al. 1999, *MNRAS*, 303, 659
- Hornschemeier, A.E., et al., 2000, *ApJ*, 541, 49
- Hughes, D., Serjeant, S., Dunlop, J., Rowan-Robinson, M., Blain, A., Mann, R.G., Peacock, J., Efstathiou, A., Gear, W., Oliver, S., Lawrence, A., Longair, M., Goldschmidt, P., Jennes, T., 1998, *Nature*, 394, 241
- Jarvis J.F., Tyson J.A., 1981, *AJ*, 86, 476
- Jarvis, R.M., MacAlpine, G.M., 1998, *AJ*, 116, 2624
- Jenness, T., 2000, JCMT Technical Report 84, <http://www.jach.hawaii.edu/JACdocs/JCMT/tr/001/84/tr0084.html>
- Lagache, G., Abergel, A., Boulanger, F., et al., 1999, *A&A* 344, 322
- Lagache, G., Puget, J.L., 2000, *A&A*, 355, 17

- Lanzetta K.M., Yahil A., Fernandez-Soto A., 1996, *Nat*, 381, 759
- Lilly, S.J., et al., 1999a, *ApJ*, 518, 641
- Lilly, S.J., et al., 1999b, in “The formation of galactic bulges” eds. by C.M. Carollo, H.C. Ferguson, R.F.G. Wyse. Cambridge, U.K. ; New York. Cambridge University Press, 1999. (Cambridge contemporary astrophysics), p.26 (astro-ph/9903157)
- Madau P., Ferguson H.C., Dickinson M.E., Giavalisco M., Steidel C.C., Fruchter A., 1996, *MNRAS*, 283, 1388
- Mann, R.G., et al., 1997, *MNRAS*, 289, 482,
- Mann, R.G., et al., 2002, *MNRAS*, in press
- Peacock et al., 2000, *MNRAS*, 318, 535
- Phillips A.C., Guzman R., Gallego J., Koo D.C., Lowenthal J.D., Vogt N.P., Faber S.M., Illingworth G.D., 1997, *ApJ*, 489, 543
- Puget, J.L., et al., 1996, *ApJL*, 305, 5
- Richards E.A., 1999, *ApJ*, 513, L9
- Richards, E., 2000, *ApJ*, 533, 611
- Richards, E.A., Kellermann, K.I., Fomalont, E.B., Windhorst, R.A., Partridge, R.B., 1998 *AJ*, 116, 1039
- Richards, E., et al., 1999, *ApJL*, 526, 73
- Rowan-Robinson, M., et al., 1997, *MNRAS*, 289, 490
- Rowan-Robinson, M., 2001, *ApJ*, 549, 745
- Rutledge R.E., Brunner R.J., Prince T.A., Lonsdale C., 2000, *ApJS*, 131, 335
- Schlegel, D.J., Finkbeiner, D.P., Davis, M., 1998, *ApJ*, 500, 525
- Scott, S., et al., 2002, *MNRAS*, in press (astro-ph/0107446)
- Serjeant, S., et al., 1997, *MNRAS*, 289, 457
- Serjeant, S., 2002 in preparation
- Serjeant, S., et al., 2002 in preparation
- Silva L., Granato G.L., Bressan A., Danese L., 1998, *ApJ*, 509, 103
- Simpson, C., Rawlings, S., Lacy, M., 1999, *MNRAS*, 306, 828
- Smail, I., Ivison, R.J., Blain, A.W., 1997, *ApJL*, 490, 5
- Smail I., Ivison R.J., Blain A.W., Kneib J.-P., 1998, *ApJ*, 507, L21
- Smail, I., Ivison, R.J., Kneib, J.-P., Cowie, L.L., Blain, A.W., Barger, A.J., Owen, F.N., Morrison, G., 1999, *MNRAS*, 308, 1061
- Sutherland W, Saunders W., 1992, *MNRAS*, 259, 413
- Thompson. R.I., Weymann, R.J., Storrie-Lombardi, L.J., 2000, *ApJ*, in press (astro-ph/0008276)
- Williams, R.E., et al., 1996, *AJ*, 112, 1335
- Wright, E.L., 1998, *ApJ* 496, 1